Water Resources Research

RESEARCH ARTICLE
10.1029/2022WR033144

Compound Coastal, Fluvial, and Pluvial Flooding During Historical Hurricane Events in the Sabine–Neches Estuary, Texas

Nahal Maymandi[1], Michelle A. Hummel[1], and Yu Zhang[1]

[1]Department of Civil Engineering, University of Texas at Arlington, Arlington, TX, USA

Key Points:

- Compound modeling of coastal, fluvial, and pluvial drivers improves flood hazard assessment during hurricane events
- Hurricanes accompanied by extended periods of rainfall cause the largest extent and longest duration of compound flooding in estuaries
- Compound modeling can inform the selection of adaptation approaches used to mitigate flooding of critical infrastructure assets

Supporting Information:

Supporting Information may be found in the online version of this article.

Correspondence to:

M. A. Hummel,
michelle.hummel@uta.edu

Citation:

Maymandi, N., Hummel, M. A., & Zhang, Y. (2022). Compound coastal, fluvial, and pluvial flooding during historical hurricane events in the Sabine–Neches Estuary, Texas. *Water Resources Research*, *58*, e2022WR033144. https://doi.org/10.1029/2022WR033144

Received 29 JUN 2022
Accepted 8 DEC 2022

Author Contributions:

Conceptualization: Michelle A. Hummel, Yu Zhang
Formal analysis: Nahal Maymandi, Michelle A. Hummel
Funding acquisition: Michelle A. Hummel, Yu Zhang
Methodology: Nahal Maymandi, Michelle A. Hummel
Project Administration: Yu Zhang
Software: Nahal Maymandi
Supervision: Michelle A. Hummel
Validation: Nahal Maymandi

Abstract When storm surge, river discharge, and rainfall occur simultaneously or in succession, they may cause compound flooding and exacerbate impacts in coastal communities. In traditional modeling approaches, these driving processes are simulated separately, leading to discrepancies between simulated and observed data and highlighting the need for coupled modeling frameworks. Here, we develop a coupled coastal–fluvial–pluvial model for the Sabine–Neches Estuary in southeastern Texas using Delft3D to simulate flood extent and depth during Hurricanes Rita, Ike, and Harvey. For each hurricane, four scenarios (i.e., coastal, fluvial, pluvial, and compound) are modeled to determine the relative contribution of each driving force to water levels across the domain. Our results reveal that tropical cyclones such as Harvey that are accompanied by extended periods of rainfall produce the largest extent and longest duration of compound flooding. Such storms also produce highly dynamic and evolving patterns of compound flooding over their duration, with multiple flood peaks that can inhibit response and recovery efforts. When simulating these storms, a coupled model can provide substantial improvements over coastal-, fluvial-, and pluvial-only models, decreasing root mean square error by 69%, 69%, and 79%, respectively. In contrast, storms with short-duration rainfall and moderate to severe storm surge produce less extensive compound flooding, which is typically dominated by coastal–pluvial interactions. Our results further highlight the potential for compound flooding at the locations of critical water infrastructure assets, suggesting the need for flood adaptation approaches that are robust to multiple types of flooding.

Plain Language Summary The combination of storm surge, river discharge, and rainfall during hurricane events can lead to compound flooding and cause devastating impacts on coastal communities. In typical flood hazard assessments, these drivers of flooding are considered separately, even though they may interact and produce more severe flooding. Understanding the interactions between flood drivers is necessary to accurately plan for and respond to future flood events. Here, we develop a coupled computer model that incorporates coastal, riverine, and rainfall processes to simulate flooding in an estuary in southeastern Texas during three historical hurricanes. The results show that interactions between coastal, riverine, and rainfall processes are all possible in the study area, although the relative dominance of each process can vary substantially depending on patterns of rainfall and wind. Storms accompanied by extended periods of rainfall cause the largest extent and longest duration of compound flooding. For these storms, the maximum flood extents and depths can only be simulated accurately using a coupled modeling approach, which provides more than a 70% reduction in error compared to models that simulate coastal, riverine, and rainfall processes separately. This research can inform local planning efforts aimed at reducing vulnerability to future flood events.

1. Introduction

Tropical cyclones pose a significant threat to populated coastal regions, leading to substantial economic costs and loss of life (Bilskie & Hagen, 2018). Although only 18% of the 310 billion-dollar disasters that have occurred in the US since 1980 were caused by tropical cyclones, these disasters account for 53% of total costs and 44% of total deaths (National Oceanic and Atmospheric Administration, 2022a). In coastal bays and estuaries, flooding associated with tropical cyclones presents a particular challenge because it may be driven by multiple mechanisms, including storm surge (coastal), river discharge (fluvial), and direct rainfall on saturated soils, impervious surfaces, and waterways (pluvial; Hinkel et al., 2014; Wuebbles et al., 2017). When these mechanisms occur simultaneously or shortly after one another, they may interact nonlinearly and, in some cases, exacerbate the resulting inundation (Zscheischler et al., 2018). For example, elevated coastal water levels can inhibit the efficient

Visualization: Nahal Maymandi, Michelle A. Hummel
Writing – original draft: Nahal Maymandi
Writing – review & editing: Michelle A. Hummel, Yu Zhang

drainage of rainfall and river discharge to the ocean, leading to a backwater effect (Y. J. Zhang et al., 2020). The frequency and severity of compound flooding could increase in the future as a result of sea-level rise (Naseri & Hummel, 2022; Santiago-Collazo et al., 2021; Sweet & Park, 2014) and changes in tropical cyclones, which are projected to become more intense (Emanuel, 2005, 2013; Sobel et al., 2016) and wetter (Emanuel, 2017; Trenberth et al., 2018) with climate change. Thus, there is a recognized need to develop more comprehensive flood risk assessment approaches that integrate coastal, fluvial, and pluvial drivers (Herdman et al., 2018).

In the past, flood hazard assessments have typically considered flood drivers separately. For example, modeling efforts meant to support emergency response and operational decision-making during hurricanes are mainly focused on storm surge hazards and do not include riverine or rainfall effects. These include probabilistic surge hazard maps produced by the National Hurricane Center using the Sea, Lake, and Overland Surges from Hurricanes (SLOSH) model (National Oceanic and Atmospheric Administration, 2022c) and real-time surge forecasts produced by the Center for Computation and Technology at Louisiana State University using the Advanced Circulation (ADCIRC) model (Center for Computation and Technology and Louisiana Sea Grant, Louisiana State University, 2022). The Federal Emergency Management Agency (FEMA)'s flood zone mapping approach also considers rainfall-runoff and storm surge processes separately (Federal Emergency Management Agency, 2016). While these approaches provide important insight into inundation potential from individual hazards, they are unable to account for nonlinear interactions caused by two-way feedback between coastal and watershed processes and have been shown to cause discrepancies between observed and modeled flood extent and depth (Bilskie et al., 2021; Kumbier et al., 2018; Loveland et al., 2021).

Recent research efforts have placed increased attention on the development of numerical modeling frameworks that can account for compound flood mechanisms in complex coastal estuaries. Santiago-Collazo et al. (2019) provide a comprehensive review of the models and coupling approaches that have been used in the literature. Briefly, coupling may occur through simple one-way linkage, where one model provides boundary condition data for another but no feedback occurs. In this case, one model must be chosen to serve as the base model for flood simulation. Depending on the application, the base model may be a hydrologic model that captures rainfall-runoff processes (Karamouz et al., 2017; Silva-Araya et al., 2018), a hydraulic model that simulates water surface profiles and velocities (Bakhtyar et al., 2020; Chen & Liu, 2014; Gori, Lin, & Smith, 2020; Wing et al., 2019), or an ocean circulation model that captures hydrodynamic and meteorological processes, such as storm surge and tides (Y. Zhang & Najafi, 2020).

Although one-way approaches are computationally efficient and provide insight into compounding effects, two-way coupling approaches are needed to simulate the complex interactions that occur at the terrestrial–coastal interface. Two-way coupling can be categorized into loosely coupled, tightly coupled, and fully coupled approaches (Goodall et al., 2011; Sulis et al., 2010). Loose coupling involves the transfer of inputs between separate models using an external interface. This approach has been applied to couple the hydrologic model pWASH123D with ADCIRC, using the Earth System Modeling Framework as the coupling interface (Campbell et al., 2010). Tight coupling removes the need for external data passage by integrating the governing equations from one model into the code of another. Tang et al. (2013) assessed coastal flood vulnerability due to sea-level rise and storms in Delaware Bay by tightly coupling a 3D ocean circulation model, a 2D shallow water model, and a topography-based hydrologic model. Fully coupled models solve the same set of governing equations to simulate all relevant processes. Recent studies have used the Semi-implicit Cross-scale Hydroscience Integrated System Model (SCHISM) as the basis for a 3D ocean-to-creek model to simulate compound coastal, fluvial, and pluvial flooding in bays along the US East and Gulf coasts (Huang et al., 2021; Ye et al., 2020, 2021; Y. J. Zhang et al., 2020). For example, Huang et al. (2021) applied SCHISM to estimate the compound and individual effects of coastal, fluvial, and pluvial forcing to water levels in and around Galveston Bay during Hurricane Harvey. However, the application of tightly or fully coupled models for compound flood hazard assessment is still limited (Santiago-Collazo et al., 2019). In addition, while many compound modeling efforts have simulated the interactions between storm surge and river discharge (e.g., Kumbier et al., 2018; Loveland et al., 2021; Xiao et al., 2021), far fewer have investigated the pluvial contribution to flooding (Gori, Lin, & Smith, 2020).

The extent and intensity of rainfall, along with its timing relative to peak storm surge, are important factors that influence the type and severity of compound flooding (Gori, Lin, & Smith, 2020). In their analysis of six tropical cyclones that impacted the Cape Fear River Estuary, Gori, Lin, and Smith (2020) concluded that rainfall occurring prior to a hurricane's landfall over extensive areas in upstream watersheds produced a peak river

discharge that coincided with the surge peak, leading to coastal–fluvial compounding effects. However, when rainfall was more localized or occurred at or after peak storm surge, coastal–pluvial compounding resulted. Despite the critical role that the timing of rainfall and surge plays in determining the severity of compound flooding, the temporal dimension of flood drivers and interactions is largely underreported in modeling studies, which often extract static grid cell or transect-based water levels to quantify compounding or transition zones (Bilskie & Hagen, 2018; Ye et al., 2021). Statistical analyses of bivariate return periods for flood drivers also typically assume that coastal surge and rainfall or river discharge peaks are coincident or occur within a specified time lag (Gori, Lin, & Xi, 2020). While this assumption may be adequate for certain storms and estuary systems, a more comprehensive analysis approach is needed to quantify the time-varying evolution of coastal, fluvial, and pluvial contributions to compound flooding across a diverse range of tropical cyclone and watershed characteristics.

Tropical cyclones pose a substantial risk to water infrastructure. Flooding can cause direct damage to water and wastewater treatment plants, while hurricane-force winds can cause power outages that prevent the pumping and treatment of raw water (Copeland, 2005; Mejia Manrique et al., 2021). Such disruptions can lead to loss of drinking water supply for homes and businesses or result in spills of untreated wastewater to nearby waterways, presenting a risk to human and ecosystem health (Schwab et al., 2007). Recovery and repair efforts are time- and resource-intensive, often taking months or years and costing millions of dollars (Copeland, 2005). During Hurricane Harvey in 2017, 40 wastewater systems and 61 public drinking water systems malfunctioned, and 203 boil-water notices were issued, some of which lasted more than 3 months (U.S. Environmental Protection Agency, 2019). In addition to the impacts on residential users, the loss of reliable water supply can also hinder commercial activities and cause cascading economic impacts (Wasileski et al., 2011). Given these risks, there is a strong incentive to mitigate impacts to critical water infrastructure to reduce future losses. However, current single-hazard planning frameworks do not provide the information needed to understand and plan for water infrastructure exposure during compound flood events.

In this study, we develop a coupled flood model using Delft3D-FM (Deltares, 2020) and apply the model to simulate hurricane-induced flood hazards in the Sabine–Neches Estuary (SNE) in southeast Texas. Our goals are to (a) evaluate the suitability of Delft3D-FM for compound coastal–fluvial–pluvial inundation modeling under tropical cyclone forcing, (b) assess how the spatial structure and temporal evolution of three historical hurricanes influence the patterns of compound flood hazards in the SNE, and (c) determine which flooding mechanisms are dominant at critical water infrastructure locations in the SNE to inform planning and hazard mitigation efforts. Our approach builds upon previous compound modeling efforts by including the effects of rainfall on the model grid and by using a single code and domain to simulate coastal, fluvial, and pluvial processes simultaneously. We also account for the time-varying evolution of compound flooding across storms events, a consideration that has been overlooked in many past studies (e.g., Huang et al., 2021). These features enable more comprehensive flood risk assessments for communities and critical infrastructure in estuarine regions.

2. Study Area

The SNE is located in southeast Texas and forms the confluence between the Sabine and Neches Rivers and the Gulf of Mexico (Figure 1). This region has been impacted by numerous tropical cyclones over the past two decades, including Hurricane Rita in 2005, Hurricane Ike in 2008, and Hurricane Harvey in 2017. These events have led to substantial flooding and damage to residents, critical infrastructure, and the economy, particularly in the two largest municipalities, Beaumont (pop. 115,282) and Port Arthur (pop. 56,039; United States Census Bureau, 2021). Water supplies for municipal, industrial, and agricultural users in the region are provided by the Lower Neches Valley Authority (LNVA). LNVA manages critical water infrastructure, including the Neches River Saltwater Barrier to control salinity and protect freshwater supplies and the North Regional Treatment Plant in Beaumont to treat industrial wastewater (Figure 1). LNVA's infrastructure has been impacted by flooding due to past storm events (Lower Neches Valley Authority, 2018), and the agency is now considering what actions are needed to build resilience to future flooding. Comprehensive flood hazard mapping that accounts for the potential for compound flooding would provide an important resource to inform this planning effort.

Several past studies have examined compound flooding along the Texas Coast using physical (Huang et al., 2021; Loveland et al., 2021; Sebastian et al., 2021), statistical (Santos et al., 2021), and combined (Couasnon et al., 2018; Liu, 2017; Muñoz, Abbaszadeh, et al., 2022) approaches. These studies have mainly focused on Galveston Bay, with less attention paid to the SNE. Recently, Loveland et al. (2021) developed a coupled framework using

Figure 1. Map of the Sabine–Neches Estuary, Texas. Red markers show the National Oceanic and Atmospheric Administration tide gauges used in this study. Blue markers show the locations of critical water and wastewater infrastructure operated by the Lower Neches Valley Authority.

ADCIRC as the base model to simulate compound coastal and fluvial flooding in the SNE during Harvey and found that including river discharges from the Neches and Sabine River watersheds was crucial to accurate flood mapping. Santos et al. (2021) explored the effect of compound flood-driven dependencies between storm surge and river discharge in Sabine Lake using statistical methods. They concluded that the 1% annual exceedance probability water level in Sabine Lake was 35 cm higher when considering dependencies between coastal and fluvial processes as compared to an independence assumption. However, none of the studies in the SNE included the direct influence of rainfall, which occurred at historic rates across the region during Harvey. Thus, the pluvial contribution to compound flood potential during Harvey and other past hurricane events is still not clear. In addition, although the interaction between surge and rainfall has often been cited as a driver of severe flooding during Harvey (Blake & Zelinsky, 2018), it remains to be seen to what extent surge contributed to observed flooding within the SNE. An analysis of the temporal evolution of coastal, fluvial, and pluvial mechanisms and their contribution to compound flood potential during Harvey is warranted given that surge and discharge in the SNE lasted for more than 3 and 7 days (Santos et al., 2021), respectively, with noncoincident peaks.

3. Methods

3.1. Model Development

We utilized Delft3D-FM (Deltares, 2020) as the computational basis to model coastal, fluvial, and pluvial processes in the SNE. Delft3D-FM is a 2D-3D hydrodynamic modeling software that is capable of modeling

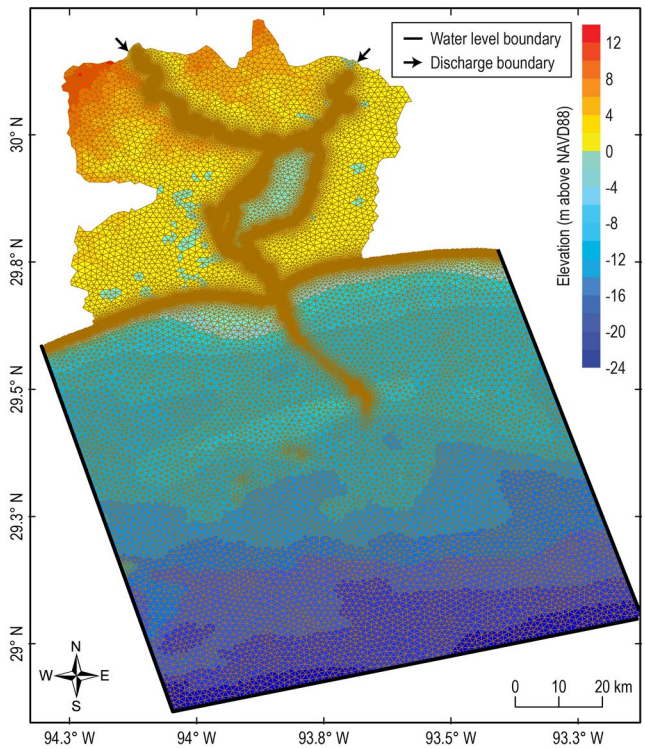

Figure 2. Model grid, topobathy, and boundary locations. The domain includes Sabine Lake, the Neches and Sabine Rivers upstream to 47 and 28 km, respectively, and part of the Gulf of Mexico.

wind, pressure, rain, river flows, surge, and tides on a single model domain and has been applied successfully in past studies of compound flooding (Bakhtyar et al., 2020; Kumbier et al., 2018; Muñoz, Moftakhari, et al., 2022; Muñoz et al., 2020). Delft3D-FM solves the Navier-Stokes equations and Boussinesq assumptions for an incompressible fluid in shallow water conditions on an unstructured grid to simulate water velocities and elevations in coastal, riverine, and estuarine systems (Veeramony et al., 2017). The model utilizes a rain-on-grid approach to ingest rainfall data as a volume source term in each grid cell at the beginning of each time step. The rainfall term P is combined with local source and sink terms to determine the total water contribution Q per unit area:

$$Q = \int_0^h (q_{in} - q_{out})\, dz + P \tag{1}$$

where q_{in} and q_{out} represent discharges and withdrawals per unit volume, respectively, and are integrated over the water depth h. Q is then incorporated into the continuity equation as follows:

$$Q = \frac{\partial h}{\partial t} + \frac{\partial U h}{\partial x} + \frac{\partial V h}{\partial y} \tag{2}$$

where U and V are depth-averaged velocities. Drying and flooding processes are simulated by adding or removing grid cells from the flow domain based on a user-defined water depth threshold (Deltares, 2022).

We applied the model in unsteady, 2D depth-averaged mode, as is common for compound flood modeling (Muñoz et al., 2020). The computational domain covered a 2,500 km^2 inland area and included Sabine Lake, the Neches and Sabine Rivers upstream to 47 and 28 km, respectively, and offshore areas extending up to 88 km into the Gulf of Mexico (Figure 2). In overland areas, the inland model boundary was defined based on hydrologic units (HUC-12). Coastal, fluvial, and pluvial forcings were fully coupled within the model domain using Delft3D-FM. However, the model did not simulate rainfall-runoff generation processes in the upstream regions of the Neches and Sabine River watersheds located outside the model boundaries. Instead, inputs from upstream watersheds were included as discharge boundaries in the Neches and Sabine Rivers. The effects of interception, infiltration, and evaporation were not modeled due to a lack of available data and based on the assumption that these effects were small compared to the influence of rainfall, as has been assumed in other studies of Harvey (Huang et al., 2021; Thyng et al., 2020).

Grid resolution varied from approximately 1,000 m offshore to 40 m nearshore and in the rivers, ship channel, and Sabine Pass, resulting in 161,623 total grid cells. Roughness was modeled using a spatially variable Manning's n based on land cover. The model was cold-started and allowed to spin up for several days prior to hurricane landfall. An adaptive time step was used for model computations based on the Courant condition (Deltares, 2022). A threshold of 10 cm was used for the drying and flooding algorithm, as has been employed in past studies (Kumbier et al., 2018).

3.2. Flood Scenarios

The model was calibrated for a nonextreme condition in January 2016 and an extreme condition during Tropical Storm Imelda in 2019 (see Section 3.4). The calibrated model was then used to simulate three historical hurricane events: Rita (2005), Ike (2008), and Harvey (2017). These three hurricanes exhibit distinct tracks and patterns of rainfall, as shown in Figure 3. Rita made landfall east of Sabine Pass on 24 September 2005, as a Category 3 hurricane with maximum sustained winds of 100 knots, a radius to maximum wind (R_{max}) of 30 nautical miles (nm), and a forward speed of 9–11.5 mph (Cooperative Institute for Research in the Atmosphere, 2021; Knabb et al., 2006). Rita produced 226 mm of total rainfall at Beaumont and a maximum surge of approximately 1.5 m at Sabine Pass (Knabb et al., 2006). Ike made landfall on Galveston Island, TX, on 13 September 2008,

10.1029/2022WR033144

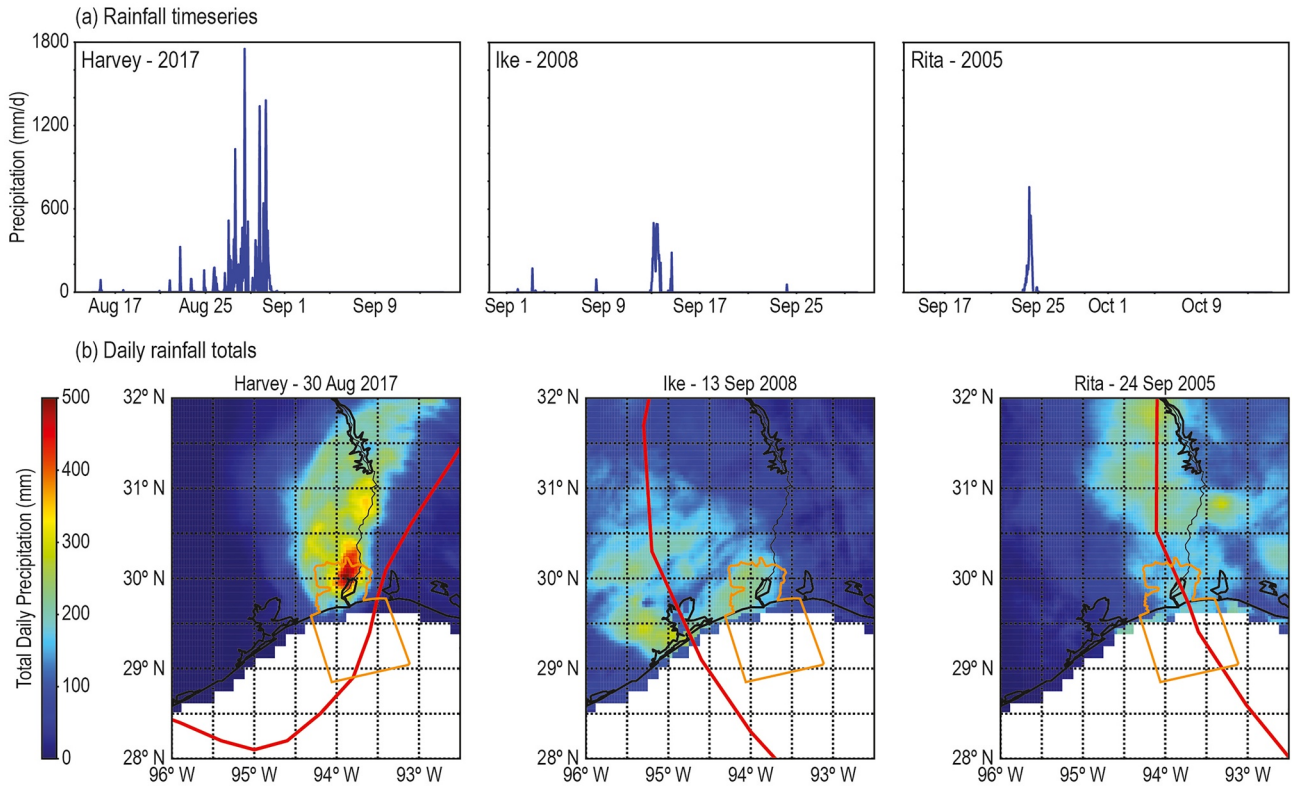

Figure 3. (a) Rainfall time series at Rainbow Bridge for Harvey, Ike, and Rita. (b) Total daily rainfall for Harvey, Ike, and Rita on the day of landfall. The orange outline indicates the limits of the study area, and the red lines show the hurricane tracks.

as a Category 2 hurricane with maximum sustained winds of 95 knots, R_{max} of 30 nm, and a forward speed of 13.5 mph (Cooperative Institute for Research in the Atmosphere, 2021; Ebad Sichani et al., 2020). Within the study area, Ike produced 138 mm of total rainfall at Beaumont and a maximum storm surge of 3.9 m at Sabine Pass (Berg, 2009). Ike caused major disruptions to the local water supply by damaging the Neches River Saltwater Barrier and allowing saltwater penetration into the upstream watershed. Harvey made landfall on 26 August 2017, near Rockport, TX, as a Category 4 hurricane with maximum sustained winds of 115 knots and R_{max} of 15 nm, then again on 30 August 2017, near Cameron, LA, as a tropical storm with maximum sustained winds of 40 knots, R_{max} of 50 nm, and a forward speed of 5–7 mph (Brown-Giammanco et al., 2018; Cooperative Institute for Research in the Atmosphere, 2021; National Weather Service, 2017). In the SNE, Harvey produced a total rainfall of 1,207 mm at the Southeast Texas Regional Airport outside Beaumont and a maximum surge of 1.0 m at Sabine Pass (Blake & Zelinsky, 2018).

3.3. Data Sources

Detailed topographic and roughness data are crucial for the accurate estimation of flooding since they control surge propagation and frictional dissipation (Federal Emergency Management Agency & US Army Corps of Engineers, 2011). Bed level and roughness values were extracted from the TX2008 ADCIRC mesh developed to support federal flood insurance studies in coastal Texas counties following Ike. Detailed information about the data sources used can be found in Federal Emergency Management Agency & US Army Corps of Engineers (2011). To summarize, offshore bathymetry for the ADCIRC mesh was derived from the National Oceanic and Atmospheric Administration (NOAA)'s depth-sounding database and navigational charts, while bathymetry for inland waterways was obtained from regional bathymetric surveys conducted by the US Army Corps of Engineers and other agencies prior to 2005. Topographic data were taken from 10-m lidar data produced by FEMA and local surveys and published in 2005 and 2006. All bathymetric and topographic data were referenced to NAVD88. Manning's n coefficients were defined based on land cover types in the National Land Cover Database (Table S1 in Supporting Information S1; U.S. Geological Survey, 2010). We made local refinements to the

Table 1
Summary of Sources Used to Generate Input Data for the Numerical Model

Period	Data	Reference
Imelda, 10 September to 30 September 2019	Neches River discharge	USGS 08041780
	Sabine River discharge	NWM
	Offshore water level	NOAA 8770822
	Rainfall	NEXRAD Stage IV
	Wind and pressure	NCEP NARR
January 2016, 1 January to 30 January 2016	Neches River discharge	USGS 08041780
	Sabine River discharge	NWM
	Offshore water level	NOAA 8770822
	Rainfall	N/A
	Wind and pressure	NCEP NARR
Harvey, 15 August to 15 September 2017	Neches River discharge	USGS 08041780
	Sabine River discharge	NWM
	Offshore water level	NOAA 8770822 and CERA
	Rainfall	MRMS
	Wind and pressure	NCEP NARR
Ike, 1 September to 30 September 2008	Neches River discharge	USGS 08041780
	Sabine River discharge	NWM
	Offshore water level	NOAA 8770570
	Rainfall	NEXRAD Stage IV
	Wind and pressure	NCEP NARR
Rita, 15 September to 15 October 2005	Neches River discharge	USGS 08041780
	Sabine River discharge	NWM
	Offshore water level	NOAA 8770570 and GTSR
	Rainfall	NEXRAD Stage IV
	Wind and pressure	NCEP NARR

ADCIRC bed level and roughness data to address anomalies. For example, the data extracted from the TX2008 ADCIRC mesh captured roughness values from land use types other than water (e.g., two bridges crossing the Neches River), which we adjusted to instead represent roughness in the river channel. Channel bed levels in the upstream reaches of the Neches and Sabine Rivers, beyond the extent of bathymetric surveys, were not well resolved in the TX2008 ADCIRC mesh. To better capture flow in the rivers, we adjusted the channel bed levels in these areas based on depth and width estimates using a simplified rectangular cross section, which was assumed to remain constant to the upstream extent of the model.

The simulation time periods and sources of meteorological and boundary forcing data for the three hurricanes and two calibration periods are summarized in Table 1. Wind and pressure fields with 3-hr temporal resolution were extracted from the National Center for Environmental Prediction (NCEP) North American Regional Reanalysis (NARR) using a mesh with a resolution of 34 by 30 km (National Center for Atmospheric Research, 2022), resulting in six horizontal and four vertical grids over the study domain. NCEP NARR wind products are derived from buoy and satellite data (National Center for Atmospheric Research, 2017). Hourly gridded rainfall time series were derived from Next Generation Weather Radar (NEXRAD) Stage IV at 4-km resolution (National Oceanic and Atmospheric Administration, 2022b). For Harvey, higher-resolution (1 km) radar-only Multi-Radar Multi-Sensor (MRMS) gridded data were used instead (Iowa Environmental Mesonet, 2022), as they provided a better fit for observed data. Hourly river discharge was extracted from USGS 08041780 Neches Rv Saltwater Barrier at Beaumont for the Neches River (U.S. Geological Survey, 2022b) and from the National Water Model

(NWM) for the Sabine River (National Science Foundation, 2019). The NWM uses MRMS hourly rainfall data to estimate flows.

Water level time series from NOAA (National Oceanic and Atmospheric Administration, 2022d) at Texas Point, Sabine Pass (8770822) were used to force the model at the offshore boundary for both calibration periods. Water level data were not available at this station during Ike and Rita, so data from NOAA Sabine Pass North (8770570) were used instead. Data from the Global Tide and Surge Reanalysis (GTSR) were used to fill gaps in the NOAA water level data during Rita (Muis et al., 2016). For the Harvey simulation, offshore water levels were extracted from Coastal Emergency Risks Assessment (CERA) hindcast modeling using ADCIRC (Center for Computation and Technology and Louisiana Sea Grant, Louisiana State University, 2022), which does not include river inputs and thus avoids capturing any fluvial signal that might result from high discharge through Sabine Pass. Because CERA data were only available from 24 August to 31 August, water levels were obtained from Texas Point, Sabine Pass (8770822) for the rest of the simulation. Water level time series from the Sabine Pass North (8770570), Port Arthur (8770475), and Rainbow Bridge (8770520) NOAA tide gauges (Figure 1) were used for model calibration and validation.

3.4. Model Calibration

We calibrated the model using two separate time periods: (a) a nonextreme condition in January 2016 to ensure that the model was accurately representing typical hydrodynamic conditions in the estuary and (b) an extreme condition with overland flooding during Tropical Storm Imelda (2019) to confirm the model's ability to capture overland flow effects. The roughness coefficient was selected to calibrate the model because friction is a significant parameter in estimating water surface elevation and velocity (Hsu et al., 1999). Roughness coefficients in the waterways were adjusted iteratively for the nonextreme January 2016 period until an acceptable match was obtained between modeled and observed water levels at the three NOAA tide gauges mentioned previously. Roughness coefficients in overland areas were then calibrated by comparing simulated water surface elevations for the extreme condition during Imelda with 30 high water marks (HWMs) available through the Dartmouth Flood Observatory (2019). We calculated the root mean square error (RMSE), coefficient of determination (R^2), Nash-Sutcliffe Efficiency (NSE), and mean absolute error (MAE) between model outputs and observations for each set of roughness coefficients to select the one that provided the best match.

3.5. Compound Flooding Decomposition

To determine the relative contribution of coastal, fluvial, and pluvial processes to tropical cyclone flooding in the SNE, we modeled four scenarios for each hurricane event: (a) coastal, (b) fluvial, (c) pluvial, and (d) compound. For the coastal scenario, offshore water levels included both tide and surge. Spatially and temporally variable wind and pressure fields were applied using gridded data. No rainfall or river discharge was included. For the fluvial scenario, offshore water levels included tides only and were derived from tidal predictions produced by NOAA using 37 tidal constituents. Hourly observed discharges were applied at the upstream extent of the Neches and Sabine Rivers. No rainfall or storm surge forcing was included. For the pluvial scenario, offshore water levels included tides only, and rainfall was applied across the whole domain. No river discharge or storm surge forcing was included. For the compound scenario, offshore water levels included both tide and surge. Gridded wind, pressure, and rainfall data were applied across the whole domain. Hourly observed discharges were applied at the upstream extent of the Neches and Sabine Rivers. For each scenario, RMSE, R^2, NSE, and MAE values were calculated to assess the ability to reproduce the observed data.

Several methods have been proposed in the literature to delineate compound or transition regions where the effects of multiple drivers interact to influence water levels (Bilskie & Hagen, 2018; Huang et al., 2021). In this study, we apply the approach outlined by Huang et al. (2021), which quantifies the relative contributions of pluvial, fluvial, and coastal forcings to peak water levels using the concept of disturbance (D). Because D can be calculated for each grid cell in the model domain, this approach provides a straightforward implementation to determine the spatial extent of the compound zone and regions where a single driver is dominant. For each flood driver, D is defined as

$$D = \begin{cases} \eta & \text{if } h \geq 0 \\ \eta + h & \text{if } h < 0 \end{cases} \quad (3)$$

where η is the water surface elevation and h is the bed level (positive downward), referenced to the same vertical datum (NAVD88; Huang et al., 2021). D represents the water depth in land areas that are initially dry and the water surface elevation in waterways that are initially wet.

For each grid cell in the model domain, we found t_{peak}, the time of maximum water level in the compound model, and calculated $D_{coastal}$ from the coastal-only model, $D_{fluvial}$ from the fluvial-only model, and $D_{pluvial}$ from the pluvial-only model at t_{peak}. Note that for Harvey, we calculated these values at two different times—one near the peak of storm surge and one near the peak of riverine discharge—to quantify the temporal changes in compound flood hazards. We then approximated the contribution C of each forcing scenario to peak water levels by calculating the ratio of the individual D to the total D at t_{peak} following the general approach proposed by Huang et al. (2021). For example, the coastal contribution ($C_{coastal}$) was calculated as

$$C_{coastal} = \frac{D_{coastal}}{D_{coastal} + D_{fluvial} + D_{pluvial}} \quad (4)$$

Although this approach does not directly capture nonlinear compound effects, it still provides insight into areas where more than one forcing may contribute at the time of peak water levels, as well as the relative importance of each forcing. The percent contribution of each forcing was also calculated at the Neches River Saltwater Barrier and the North Regional Treatment Plant to determine the main contributors to flooding at LNVA facilities.

4. Results

4.1. Model Calibration

The modeled water level results for the January calibration period are plotted alongside the observed water levels at the three NOAA tide gauges in Figure 4. Calibrated roughness values in the waterways range from $n = 0.013$ to 0.015 in Sabine Pass, Sabine Lake, and the Sabine River, $n = 0.020$ in the ship channel and offshore, and $n = 0.030$ in the Neches River. The model is able to predict the observed water levels well, with average $R^2 = 0.91$, RMSE = 0.10 m, NSE = 0.78, and MAE = 0.08 m. However, water levels are slightly overpredicted at Rainbow Bridge, possibly due to the higher level of uncertainty in the Neches River bathymetric data used to create the model. During Tropical Storm Imelda, a roughness value of $n = 0.200$ in the overland areas of the Neches River floodplain provides the best correlation with observed HWMs ($R^2 = 0.87$, RMSE = 0.19 m, NSE = 0.81, and MAE = 0.10 m; Figure 5a). For 84% of the HWMs, modeled water depths were within ±0.2 m of observed water depths (Figure 5b). Roughness values in overland areas in the rest of the domain did not influence water levels at observation points and thus were not changed from the original spatially variable values assigned based on land use.

4.2. Hurricane Harvey

Figure 6 shows the modeled versus observed water level time series for the coastal, fluvial, pluvial, and compound scenarios during Harvey. Model performance metrics (averaged across all three NOAA tide gauges) for each scenario are summarized in Table 2. Individual performance metrics at each tide gauge are provided in Tables S2–S5 in Supporting Information S1. The coastal model matches the observed water levels well until 29 August, when the river influence begins to increase, first at the upstream station near Rainbow Bridge, then at Port Arthur, and finally at Sabine Pass. During this time, a compound effect is visible as the coastal model begins to underpredict the compound model results. The increasing riverine influence lasts for over a week at all stations, although its magnitude is attenuated further downstream near the estuary entrance as some of the fluvial inflow is converted into overland discharge east of Sabine Lake. Elevated river water levels are driven by heavy rainfall in the Neches and Sabine River watersheds starting on 27 August and extending through 30 August (Figures 3a and 3b; Figure S1 in Supporting Information S1), with daily rainfall totals exceeding 400 mm on 30 August. Even after the initial surge passes, simulations that include only the coastal influence or the fluvial influence

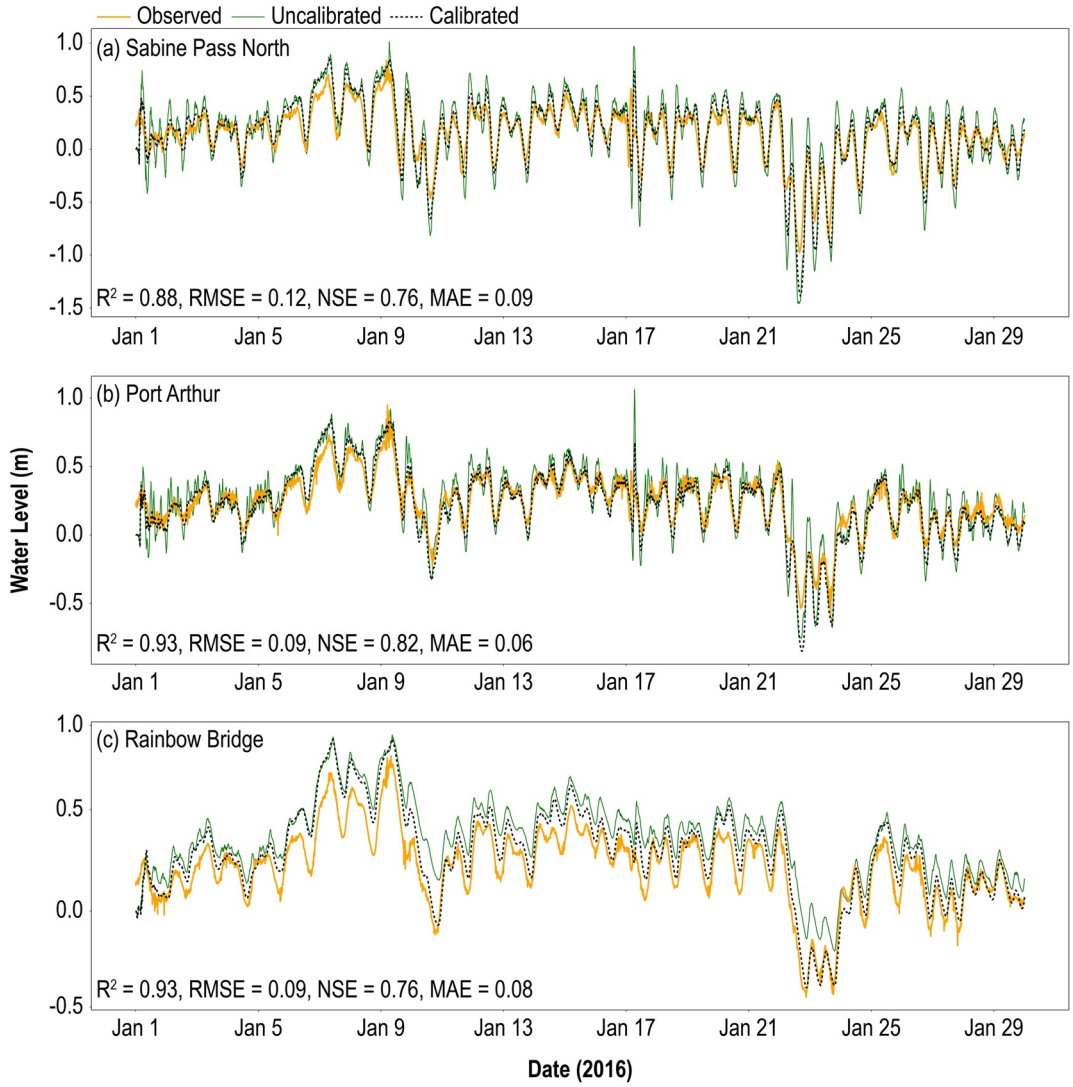

Figure 4. Modeled versus observed water levels for the January 2016 compound scenario (before and after calibration). Performance metrics are provided for the calibrated model. R^2, coefficient of determination; RMSE, root mean square error (m); NSE, Nash-Sutcliffe Efficiency; MAE, mean absolute error (m).

substantially underpredict the observed water levels at all stations, again indicating compound effects due to the interactions between these two processes. The rainfall effect is greatest at the upstream station in the watershed but is still visible at Sabine Pass. The compound flood model predicts the observed values well (Table 2; $R^2 = 0.94$, RMSE = 0.09 m, NSE = 0.91, and MAE = 0.07 m), although it does cause overprediction of water levels at Sabine Pass in the days following landfall. The compound model generally shows good agreement ($R^2 = 0.80$) with HWMs collected after Harvey (Figure 5c), although overprediction does occur at some HWM locations outside the Neches River floodplain (Figure 5d).

To further assess the importance of coastal, fluvial, and pluvial forcing across the domain during Harvey, the relative contribution of each forcing to peak water levels based on the disturbance factor is plotted for two points in time: (a) at 13:00 on 30 August, as the storm surge was receding and the fluvial influence was increasing (Figures 7a–7c), and (b) at 0:00 on 4 September, during the peak fluvial discharge (Figures 7e–7g). The timing of peak water levels is plotted in Figure 8a. On 30 August, water levels peak offshore (Figure 8a), where coastal surge is dominant (Figure 7a). Surge contributes approximately 50% to water levels in Sabine Lake and in overland areas near Sabine Pass and east of Sabine Lake. Surge also affects areas in the Neches and Sabine River watersheds to a lesser extent (Figure 7a). Fluvial processes are dominant at the upstream end of the Neches River,

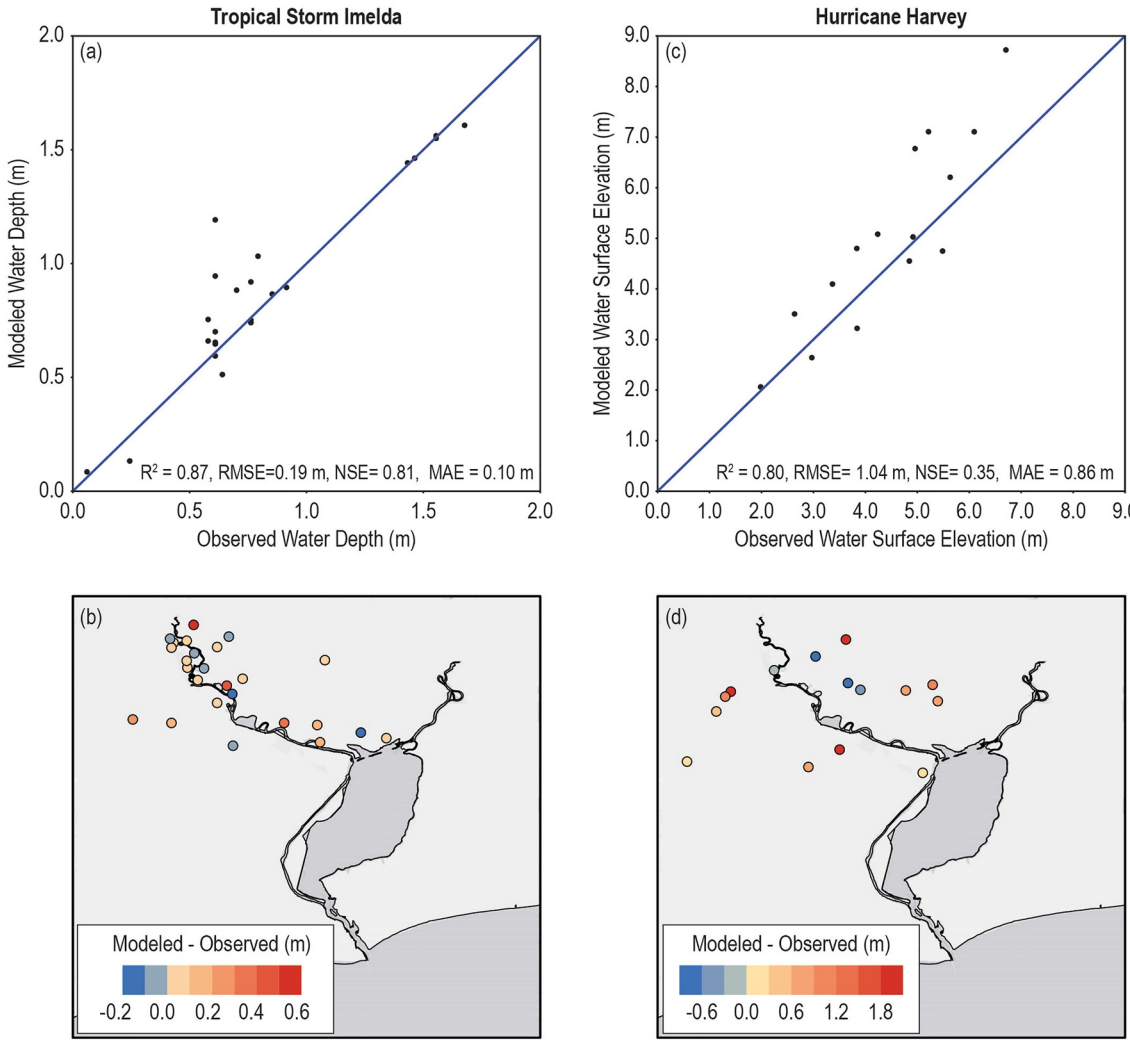

Figure 5. Comparison of (a) modeled and observed water depths at locations of high water marks for Tropical Storm Imelda (Dartmouth Flood Observatory, 2019) and (c) modeled and observed water surface elevation at locations of high water marks for Hurricane Harvey (U.S. Geological Survey, 2022a) using the calibrated compound model. Maps show the difference between modeled and observed values for (b) Imelda and (d) Harvey. R^2, coefficient of determination; RMSE, root mean square error (m); NSE, Nash-Sutcliffe Efficiency; MAE, mean absolute error (m).

as discharge begins to increase, and contribute 30%–50% to water levels in the rivers and 20% to water levels in Sabine Lake (Figure 7b). Rainfall is dominant outside the river floodplains and contributes partially (40%–50%) to water levels in overland areas adjacent to Sabine Pass, Sabine Lake, and the river channels (Figure 7c). Rainfall also contributes (20%–30%) to water levels in the waterways. Classifying the dominant forcing in each grid cell using an 80% threshold as suggested by Ye et al. (2021) (Figure 7d), it is clear that compounding effects are widespread within the waterways, from Sabine Pass to the upstream portions of the Neches and Sabine Rivers, on 30 August. During this time, coastal, fluvial, and pluvial processes all contribute to modeled water levels. Compound zones are also observed in some overland areas around Sabine Pass, east of Sabine Lake, and in small parts of the Neches and Sabine River floodplains. In these locations, coastal–pluvial interactions are the main source of flooding, although coastal–fluvial interactions are observed at the upstream end of the Neches River.

On 4 September, water levels reach their peak values in Sabine Pass, Sabine Lake, the Neches and Sabine Rivers and floodplains, and the area east of Sabine Lake (Figure 8a). Coastal processes are again dominant offshore and contribute partially to peak water levels in Sabine Pass (30%–60%) and Sabine Lake (10%–20%; Figure 7e). The fluvial influence is dominant in the Neches and Sabine Rivers and floodplains and in Sabine Lake (80%–100%; Figure 7f). Fluvial effects are also a significant contributor to peak water levels in the region east of Sabine Lake (50%–90%), as high water levels in Sabine Lake led to overflows across the eastern part of the domain. Rainfall

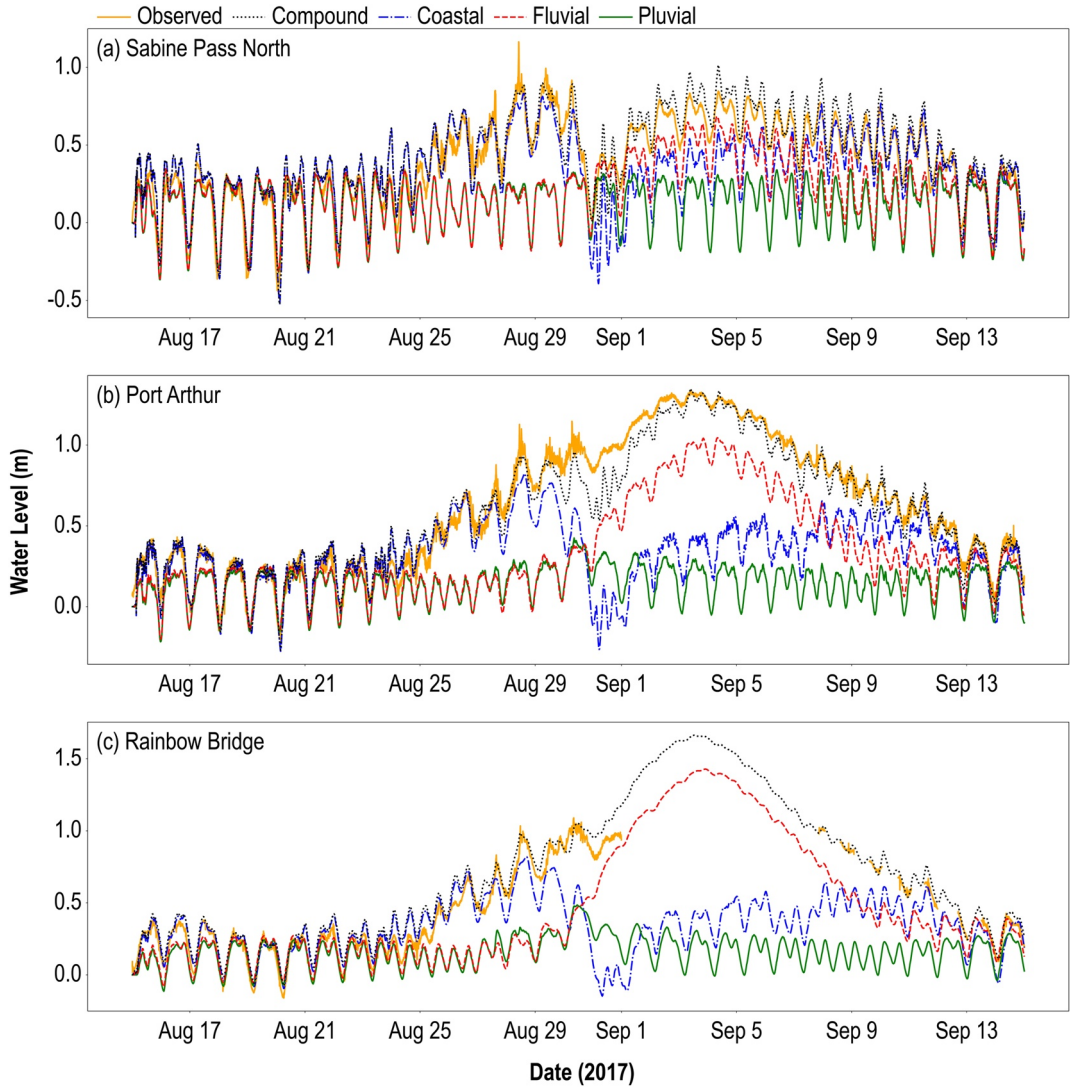

Figure 6. Modeled versus observed water levels at (a) Sabine Pass North, (b) Port Arthur, and (c) Rainbow Bridge for Hurricane Harvey.

also contributes partially to peak water levels east of Sabine Lake and in parts of the Neches and Sabine River floodplains (20%–50%; Figure 7g). Given that rainfall in the study region concludes by 31 August (Figure 3), this pluvial contribution is likely due to a lack of infiltration and drainage, which leads to ponding in overland areas. Rainfall is also dominant outside the river floodplains to the north and west of the study domain. As shown in the dominant forcing map for 4 September (Figure 7h), the compounding zone at the time of peak discharge covers much of the overland area east of Sabine Lake and smaller areas in the river floodplains and is driven by interactions between fluvial and pluvial processes. A second compound zone occurs in Sabine Pass and the downstream portions of Sabine Lake and the ship channel due to coastal–fluvial interactions.

4.3. Hurricane Ike

The modeled and observed water level comparisons for Ike are shown in Figure 9. Coastal surge is the primary contributor to peak water levels at all stations. As a result, the coastal-only model generally simulates the observations well, although it slightly overpredicts the peak water levels at Sabine Pass and Rainbow Bridge and the recession limb at all stations. A slight water level increase due to rainfall can be observed at Port Arthur and Rainbow Bridge on 13 September, when rainfall intensity is greatest across the Neches and Sabine River

Table 2
Summary of Average Model Performance Compared to Observations for Hurricanes Harvey, Ike, and Rita

Hurricane	Scenario	R^2	RMSE (m)	NSE	MAE (m)
Harvey	Compound	0.94	0.09	0.91	0.07
	Coastal	0.37	0.30	0.15	0.19
	Fluvial	0.59	0.30	0.14	0.23
	Pluvial	0.28	0.44	−0.78	0.34
Ike	Compound	0.97	0.15	0.93	0.10
	Coastal	0.96	0.14	0.94	0.10
	Fluvial	0.03	0.66	−0.30	0.36
	Pluvial	0.06	0.66	−0.31	0.37
Rita	Compound	0.86	0.10	0.83	0.08
	Coastal	0.85	0.10	0.82	0.07
	Fluvial	0.22	0.26	−0.10	0.18
	Pluvial	0.21	0.27	−0.22	0.20

Note. The reported values for each scenario are averaged across the three NOAA tide gauges (Sabine Pass North, Port Arthur, and Rainbow Bridge). R^2, coefficient of determination; RMSE, root mean square error; NSE, Nash-Sutcliffe Efficiency; and MAE, mean absolute error.

watersheds (Figures 3a and 3b). Although all three forcings peak on the same day, the fluvial and pluvial influences are negligible compared to the extreme influence of coastal storm surge. The compound flood model performs well (Table 2; average R^2 = 0.97, RMSE = 0.15 m, NSE = 0.93, and MAE = 0.10 m) but causes slight overprediction as water levels peak and recede.

Peak water levels across much of the region during Ike were dominated by storm surge (Figure 10a). This includes all areas within 30–55 km of the coastline, Sabine Lake, and the Neches and Sabine River floodplains, as surge propagated to the upstream extents of the current model domain on 13 September and into the early hours of 14 September (Figure 8b). The fluvial influence was not dominant at any location in the domain and only contributed minimally to peak water levels (Figure 10b). Rainfall was the dominant factor in the inland areas north and west of Sabine Lake (Figure 10c), although the total depth of rainfall-driven flooding in these areas was minor (average water depth = 0.4 m). Peak water levels in overland areas generally occurred on 13 September along with maximum rainfall, although some areas experienced water level maxima on 15 September due to a second period of rainfall (Figures 3 and 8b). The compound region for Ike is small and only occurs at the inland extent of the storm surge effect (Figure 10d).

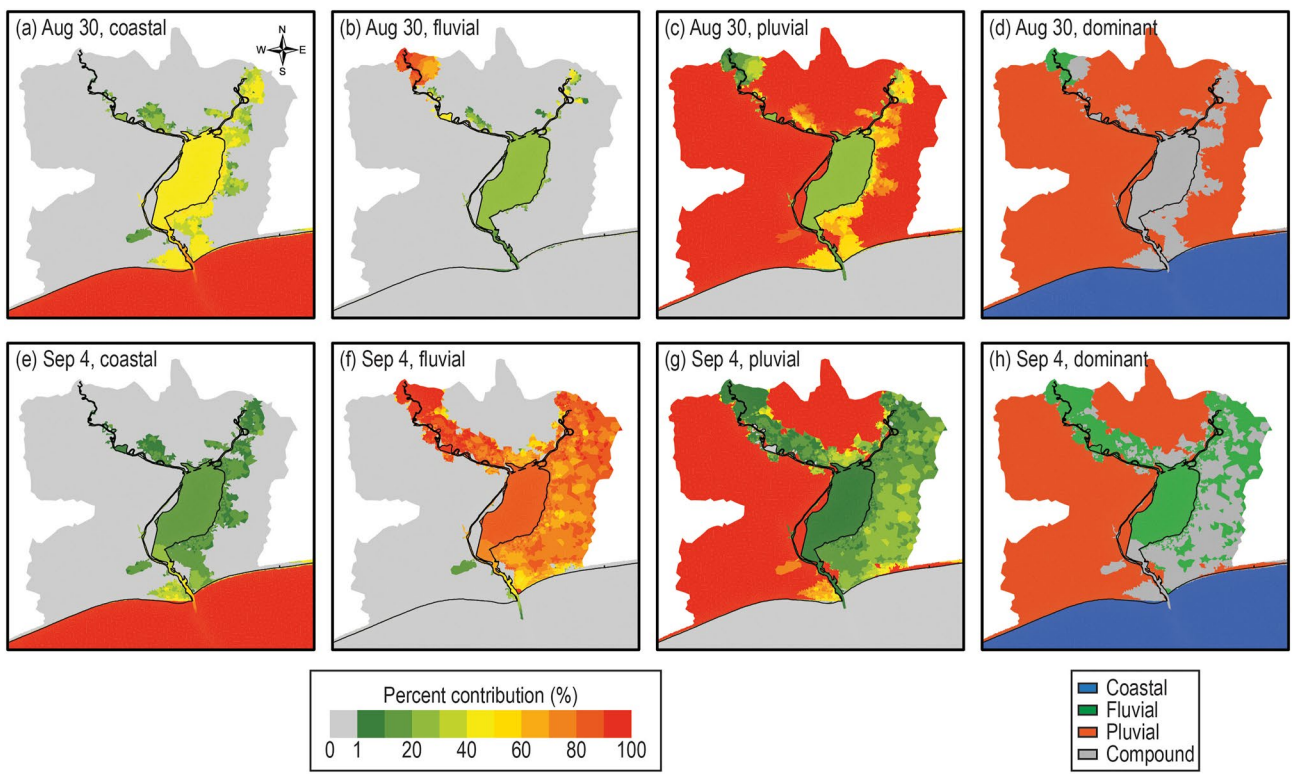

Figure 7. Percent contribution of (a, e) coastal, (b, f) fluvial, and (c, g) pluvial forcing to peak water levels for Hurricane Harvey at 13:00 on 30 August (top row) and at 0:00 on 4 September (bottom row). The dominant forcing, representing at least 80% of the peak water level, during each time period is shown in panels (d) and (h). Areas in blue are dominated by coastal influence, areas in green by fluvial influence, and areas in orange by pluvial influence. Gray areas represent locations where no forcing contributes more than 80% to the peak water levels, suggesting the potential for compound effects. The legend on the left corresponds with panels (a)–(c) and (e)–(g). The legend on the right corresponds with panels (d) and (h).

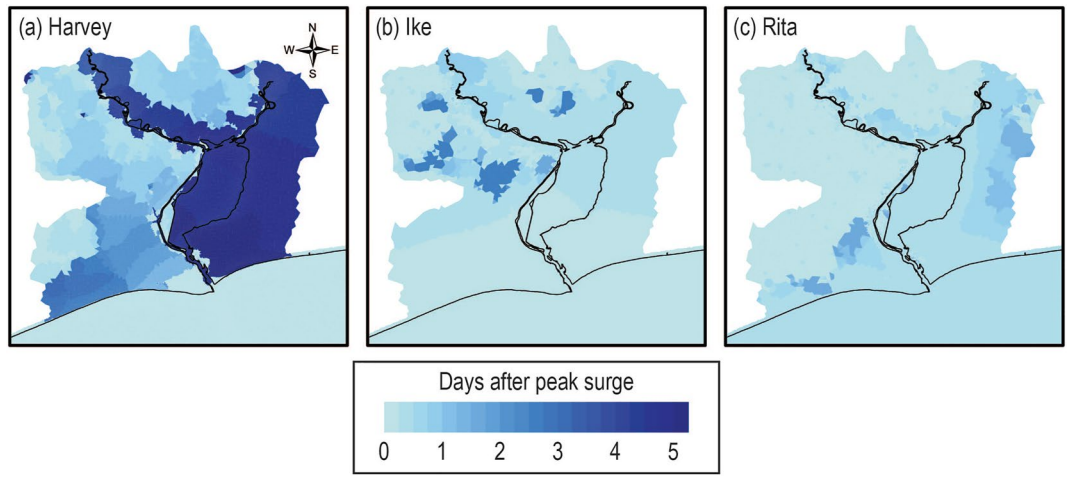

Figure 8. Timing of peak water levels for (a) Harvey, (b) Ike, and (c) Rita. Timing is shown as days after peak storm surge, which occurred at approximately 0:00 on 30 August 2017, for Harvey; 6:00 on 13 September 2008, for Ike; and 6:00 on 24 September 2005, for Rita.

4.4. Hurricane Rita

Figure 11 shows the water level comparisons for Rita. Water levels begin to increase on 23 September and remain elevated for several days after the maximum surge on 24 September. Before water levels return to prestorm conditions, a second, smaller peak is observed during the first week of October. Both peaks appear to be driven primarily by coastal influences, as the coastal-only model shows the best agreement with the observed water levels. The compound model provides good agreement with observations (Table 2; average $R^2 = 0.86$, RMSE = 0.10 m, NSE = 0.83, and MAE = 0.08 m) and performs slightly better than the coastal-only model during the recession limb of the first peak at Port Arthur and Rainbow Bridge. However, it leads to poorer performance during the second, smaller peak at Rainbow Bridge. A small rainfall effect is seen on 24 September, when rainfall intensity peaks across the domain and in the upstream watersheds (Figures 3a and 3b). In contrast to Harvey, this rainfall spike is coincident with the peak storm surge, suggesting the potential for compounding effects. A minor fluvial effect due to rainfall in the upstream watershed is visible on 30 September (several days after landfall and peak rainfall) at Rainbow Bridge and Port Arthur. However, as with Ike, the fluvial and pluvial effects are minor compared to the coastal contribution at all three gauged locations.

Rainfall is again dominant in inland areas outside the floodplains (Figure 12c), where water levels peak along with rainfall early on 24 September (Figure 8c). The average water depth due to rainfall in these areas is 0.3 m. Coastal surge propagates inland midday on 24 September (Figure 8c) and is the primary contributor to peak water levels offshore and in Sabine Lake (Figure 12a). Coastal effects also extend upstream into the river floodplains and east of Sabine Lake, generally representing 40%–80% of peak water levels. Rainfall contributes 10%–50% to flooding east of Sabine Lake (Figure 12c), where water levels peak late on 24 September through 25 September (Figure 8c). As with Ike, the riverine influence during Rita is negligible, contributing a maximum of only 10% to peak water levels (Figure 12b). Compounding effects primarily occur along the inland extent of the storm surge, in parts of the river floodplains, and east of Sabine Lake due to surge and rainfall (Figure 12d).

4.5. LNVA Water Infrastructure Assets

As mentioned previously, LNVA operates critical water infrastructure that supports municipal, industrial, and agricultural customers in the region. To examine the effects of hurricane-driven flooding on LNVA assets, we extracted the disturbance factor for each forcing at the time of peak water level in the compound scenario from the grid cells closest to the locations of the Neches River Saltwater Barrier and the North Regional Treatment Plant (Table 3). At the Saltwater Barrier, fluvial effects are dominant (97%) for Harvey, while coastal effects are dominant (78%) for Ike. Both coastal (55%) and fluvial (35%) processes contribute to peak water levels at the Saltwater Barrier during Rita. Across all storms, the pluvial effect is minimal. In contrast, at the North Regional Treatment Plant, compounding effects due to all three forcings were observed during each storm. The fluvial

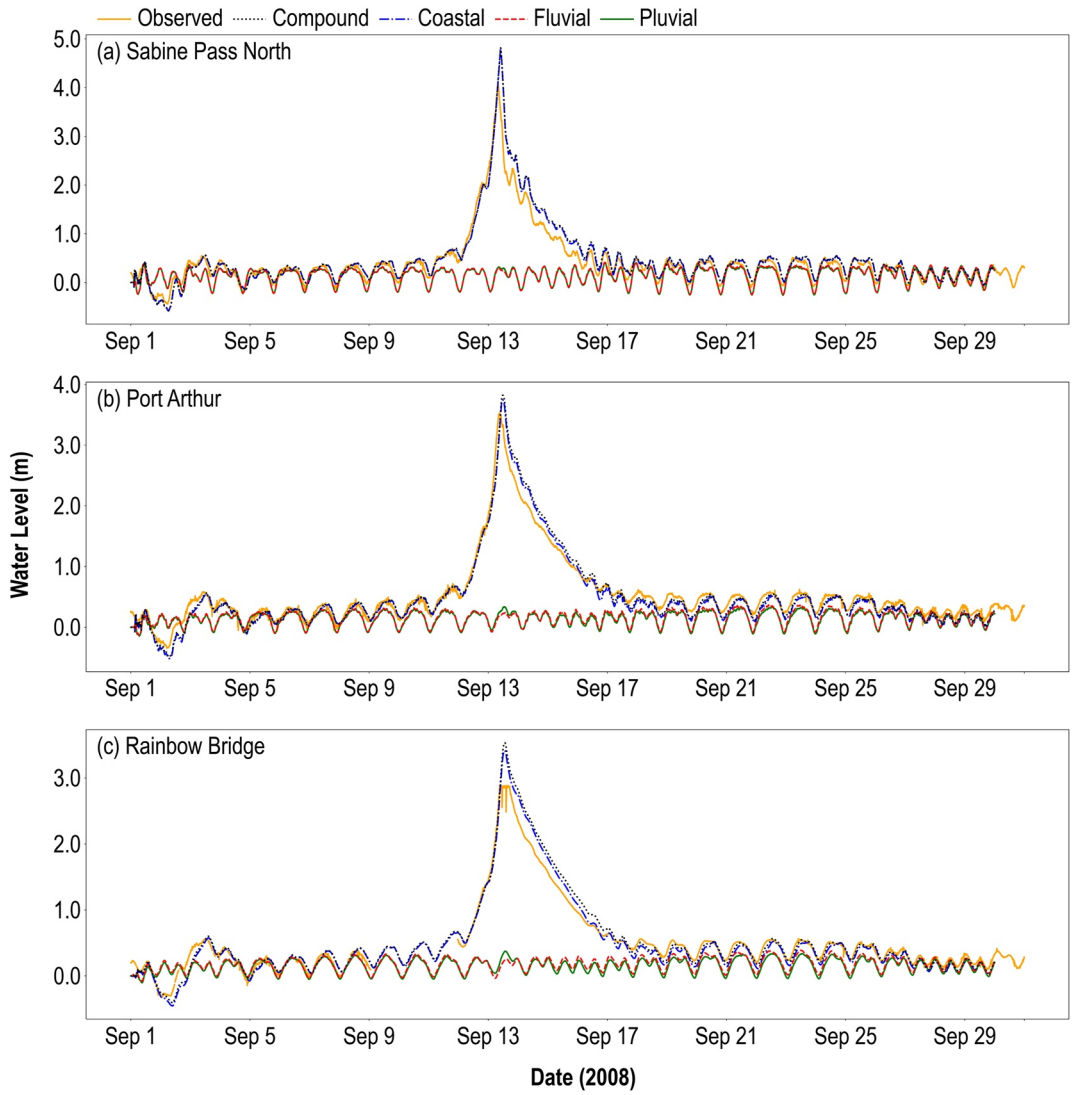

Figure 9. Modeled versus observed water levels at (a) Sabine Pass North, (b) Port Arthur, and (c) Rainbow Bridge for Hurricane Ike.

scenario contributed most during Harvey (60%), the coastal scenario during Ike (55%), and the pluvial scenario during Rita (40%).

5. Discussion

The Delft3D-FM computational engine provides a means to simulate coupled coastal, fluvial, and pluvial processes within the computational domain. The compound model was generally able to predict observed water levels well across all three hurricanes, even given their disparate meteorological characteristics. For Harvey, the compound scenario provided a significant improvement over the individual forcing scenarios at the NOAA observation stations, reducing RMSE by 0.21 m compared to the coastal and fluvial scenarios and 0.35 m compared to the pluvial scenario (Table 2). In contrast, the compound scenario provided negligible improvements over the coastal scenario at NOAA stations during Ike and Rita, since the coastal influence was dominant in Sabine Lake and the Neches River during these storms (Figures 10 and 12d). However, compounding effects were important in other parts of the domain, including in overland areas near the extent of surge penetration and east of Sabine Lake, indicating the value of using a coupled approach.

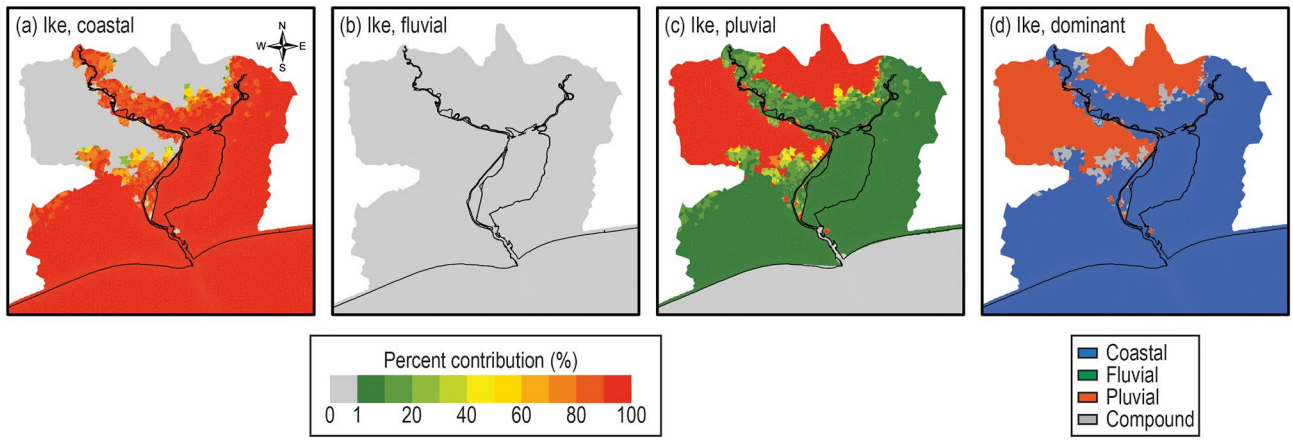

Figure 10. Percent contribution of (a) coastal, (b) fluvial, and (c) pluvial forcing to peak water levels for Hurricane Ike. The dominant forcing, representing at least 80% of the peak water level, is shown in panel (d). Areas in blue are dominated by coastal influence, areas in green by fluvial influence, and areas in orange by pluvial influence. Gray areas represent locations where no forcing contributes more than 80% to the peak water levels, suggesting the potential for compound effects. The legend on the left corresponds with panels (a)–(c). The legend on the right corresponds with panel (d).

Comparing the results of our scenario modeling for Harvey, Ike, and Rita, we observe four compound flood mechanisms in the SNE during tropical cyclone events: (a) coastal–fluvial–pluvial interactions in the waterways, (b) coastal–fluvial interactions in the downstream part of the estuary near Sabine Pass, (c) fluvial–pluvial interactions in overland areas east of Sabine Lake, and (d) coastal–pluvial interactions in overland areas east of Sabine Lake. The first mechanism occurred on 30 August 2017, as Harvey made landfall east of the SNE as a tropical storm with moderate wind speeds. Harvey's storm surge coincided with ongoing heavy rainfall over the SNE and was exacerbated by increasing river discharges following almost a week of heavy rainfall in upstream watersheds. This led to coastal–fluvial–pluvial interactions in the waterways, from Sabine Lake upstream to the Neches and Sabine Rivers (Figure 7).

The second mechanism was also observed during Harvey but occurred several days later, on 4 September 2017. Extreme rainfall falling over multiple days across the study area and in upstream watersheds during Harvey led to extensive runoff draining into the Neches and Sabine Rivers and Sabine Lake. The resulting fluvial discharge interacted with elevated coastal water levels, unrelated to the initial surge, to produce compound flooding in Sabine Pass and the downstream portions of Sabine Lake and the ship channel (Figure 7).

The third mechanism, compounding due to fluvial–pluvial interactions, was observed during Harvey in overland areas east of Sabine Lake. Peak river discharge on 4 September 2017, led to outflows from Sabine Lake that interacted with saturated and undrained conditions in overland areas impacted by extreme rainfall, causing widespread flooding. Although the peak river discharge did not coincide with the period of rainfall, the antecedent saturated conditions exacerbated the flooding caused by fluvial outflows. The influence of fluvial flows on flooding east of Sabine Lake during Harvey was also demonstrated by Loveland et al. (2021) when comparing their coastal-only scenario to a scenario that included both coastal and fluvial inputs.

Finally, the fourth mechanism occurred during both Harvey and Rita as coastal and pluvial drivers interacted. During Harvey, the initial storm surge led to overflows near Sabine Pass, east of Sabine Lake, and in small portions of the river floodplains on 30 August 2017. This coincided with heavy rainfall over the SNE, leading to concurrent coastal and pluvial impacts in limited areas. Coastal–pluvial interactions were more notable during Rita, which made landfall east of Sabine Pass as a Category 3 hurricane, with strong onshore winds driving storm surge into the estuary. Elevated water levels in Sabine Lake due to storm surge led to outflows to the east, where the pluvial effect was also high, causing a compounding effect. Coastal–pluvial compounding also occurred to a lesser extent in the river floodplains during Rita.

Based on these four mechanisms, we conclude that rainfall duration plays an important role in determining the likelihood of experiencing multiple types of compound flooding during a single storm. Tropical cyclones like Harvey that make landfall at the tail-end of an extended period of rainfall over the estuary and upstream watersheds are of particular concern, as they have the potential to produce temporal compounding with an initial

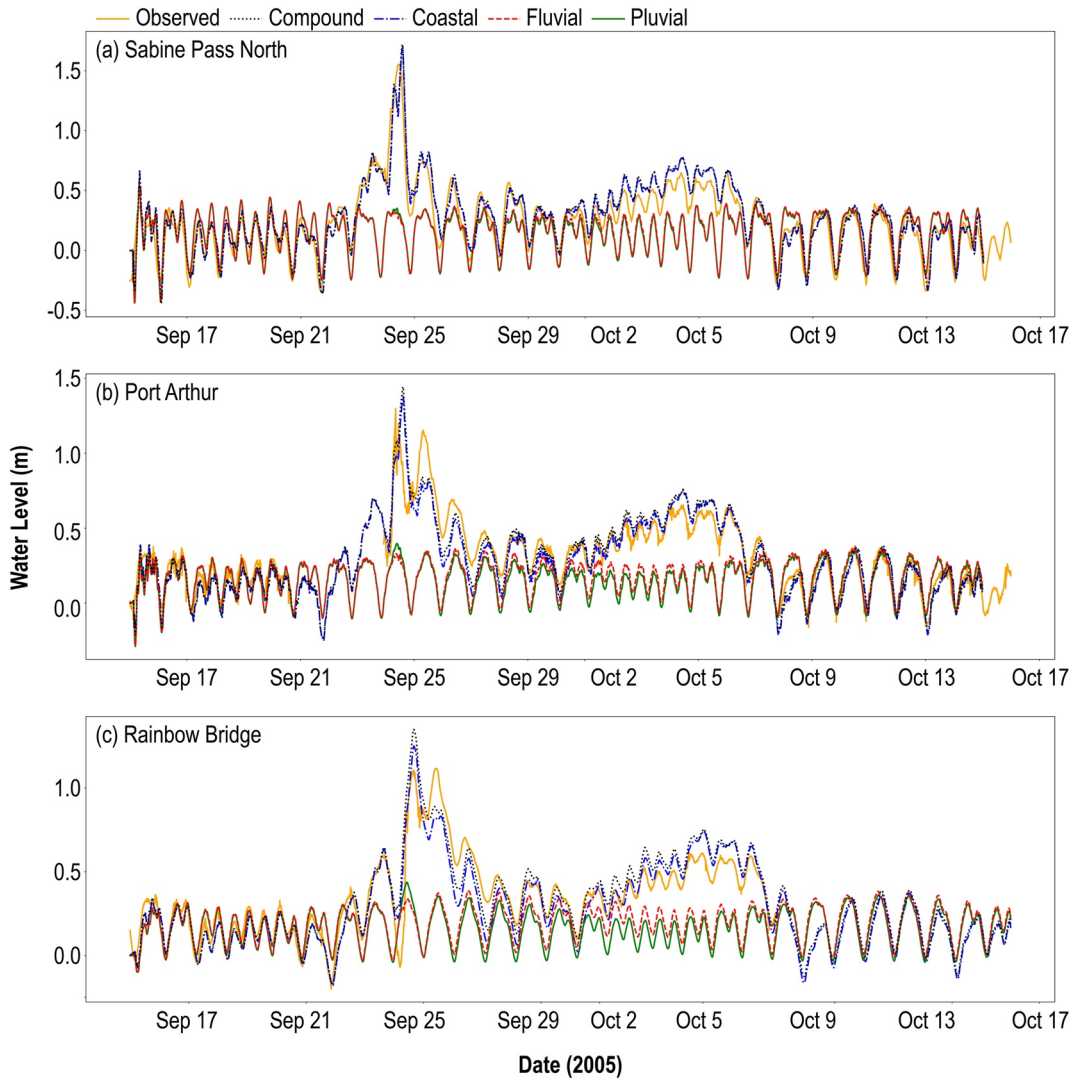

Figure 11. Modeled versus observed water levels at (a) Sabine Pass North, (b) Port Arthur, and (c) Rainbow Bridge for Hurricane Rita.

surge-driven peak followed by a lagged fluvial peak. If this lagged fluvial peak occurs before the downstream watershed has time to drain or if it coincides with a subsequent period of high coastal water levels, compounding between fluvial–pluvial or fluvial–coastal drivers can result. Such events should be carefully accounted for in emergency planning efforts so residents are aware that, even after the passing of the hurricane and associated surge, river discharge into the estuary can produce a second, potentially more severe flood peak and further delay recovery efforts. In contrast, storms like Rita that cause intense but short-duration or localized rainfall and moderate surge are likely to produce only coastal–pluvial compounding, as the fluvial influence from the Neches and Sabine Rivers will be small.

This study highlights the diversity of hazards that the SNE may face due to tropical cyclone events and suggests the need for more comprehensive flood hazard assessments that account for multiple flood drivers and their interactions. Building resilience to multiple flood drivers is particularly important for LNVA given the critical role that LNVA assets serve in maintaining surface water quality and supplies in the region. At facilities such as the North Regional Treatment Plant, protective barriers like levees or seawalls can mitigate the effects of coastal and fluvial flooding but may exacerbate the impacts of pluvial flooding by restricting off-site drainage. Dual approaches that couple protective infrastructure with pumps may be needed to effectively manage these multiple sources of flooding. Deployment of gauges to collect data on rainfall, soil moisture, and infiltration in overland

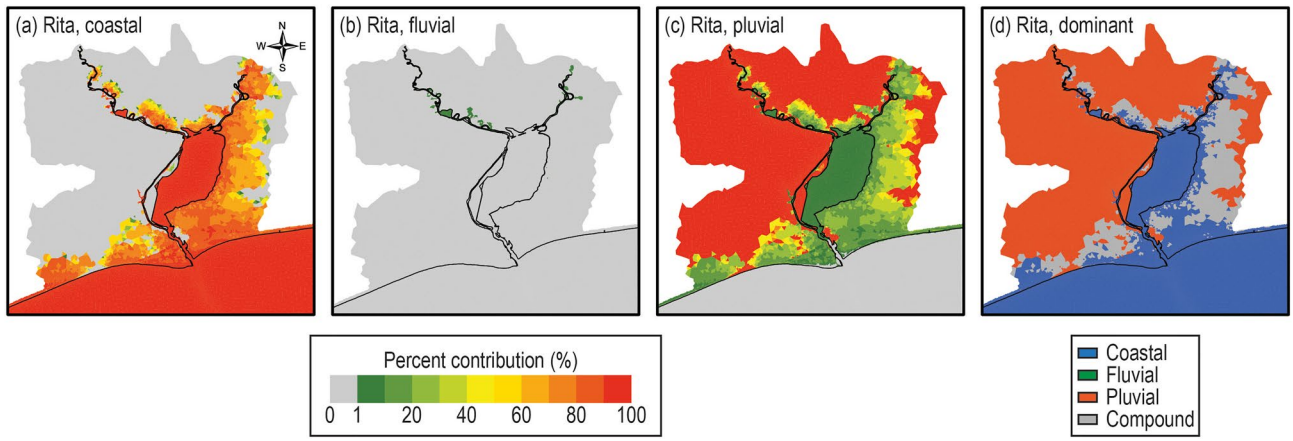

Figure 12. Percent contribution of (a) coastal, (b) fluvial, and (c) pluvial forcing to peak water levels for Hurricane Rita. The dominant forcing, representing at least 80% of the peak water level, is shown in panel (d). Areas in blue are dominated by coastal influence, areas in green by fluvial influence, and areas in orange by pluvial influence. Gray areas represent locations where no forcing contributes more than 80% to the peak water levels, suggesting the potential for compound effects. The legend on the left corresponds with panels (a)–(c). The legend on the right corresponds with panel (d).

areas could further constrain the role of pluvial flooding to inform mitigation activities. Given the potential for both coastal and fluvial impacts at the Neches River Saltwater Barrier, as demonstrated here, refined modeling of coastal–fluvial interactions and salinity distributions would provide insight into potential impacts on structural and mechanical components and upstream freshwater supplies.

6. Limitations

Detailed bathymetric survey data were only available up to the extent of dredging in the Neches and Sabine Rivers, so river cross sections further upstream were simplified within the model. This introduced uncertainty in the modeling of water levels and velocities in the upstream reaches of these rivers. In addition, the topography and bathymetry data sets used to construct the model were mostly collected prior to 2006. As a result, changes due to natural or anthropogenic influences between the three simulated hurricane events were not captured.

The data and assumptions used when implementing rainfall in the model could also cause discrepancies between modeled and observed water levels. Although 1-km resolution MRMS data were available for Harvey, only 4-km resolution Stage IV data were available for Rita and Ike, limiting the ability to capture high-resolution variability in the spatial distribution of rainfall. In addition, if the effects of interception, infiltration, or evaporation are not negligible, as was assumed in this and other studies of Harvey (e.g., Huang et al., 2021), water levels may be over-predicted. In fact, ignoring these processes may have contributed to the overprediction of water levels at HWMs outside the Neches River floodplain, where the pluvial influence was dominant during Harvey (Figure 5d). A lack of high-resolution information on antecedent soil moisture conditions and infiltration rates thus presents a challenge for accurate modeling of rainfall-runoff processes in compound flood frameworks and could be a target for future data collection efforts.

Table 3
Percent Contribution of Individual Forcing Scenarios to Peak Water Levels at LNVA Facilities

Location	Hurricane	Time of compound peak	Coastal	Fluvial	Pluvial
Neches River Saltwater Barrier	Harvey	2 Sep 2017 04:06:00	3	97	0
	Ike	14 Sep 2008 12:54:00	78	13	9
	Rita	24 Sep 2005 18:48:00	55	35	10
North Regional Treatment Plant	Harvey	2 Sep 2017 19:54:00	14	60	26
	Ike	13 Sep 2008 19:18:00	55	18	27
	Rita	25 Sep 2005 12:00:00	30	30	40

Uncertainty in the data sets used to set the model boundary conditions is another possible source of error (Abbaszadeh et al., 2022). For most scenarios, we used NOAA tide gauge data at the offshore boundary and USGS discharge data at the upstream Neches River boundary. In past studies, NOAA data were reported to have high accuracy, with errors of approximately 1 mm (Asher et al., 2019; Muñoz, Abbaszadeh, et al., 2022), although errors may be higher during extreme events (National Oceanic and Atmospheric Administration, 2013). The quality of USGS discharge measurements can range from <2% error (excellent) to >8% error (poor; Muñoz, Abbaszadeh, et al., 2022; U.S. Geological Survey, 2011). For the scenarios that used modeled data from CERA or GTSR to force the offshore boundary instead of NOAA observations, errors could result from grid resolution and input data quality. However, the data sets obtained from CERA (based on ADCIRC) and GTSR (based on Delft3D-FM) have been shown in the past to provide accurate coastal water level data to inform coastal flood studies (Dietrich et al., 2012; Muis et al., 2016). To address concerns with data accuracy and eliminate the need for observed or modeled data at the offshore boundary, the domain could be extended to cover the entire Gulf of Mexico and part of the Atlantic Ocean, thus enabling the use of hurricane wind and pressure data to generate coastal water levels offshore of Sabine Pass.

7. Conclusions

In this study, we developed a coupled flood model to investigate the potential for compound flooding in the SNE during three historical hurricane events (Harvey, Ike, and Rita). We used this model to assess the individual and combined effects of coastal, fluvial, and pluvial flood drivers on peak water levels in the study region. Our results reveal that tropical cyclones such as Harvey that are accompanied by extended periods of rainfall produce the largest extent and longest duration of compound flooding. Such storms also produce highly dynamic and evolving patterns of compound flooding over their duration, with multiple flood peaks that can inhibit response and recovery efforts. For such storms, a compound model that is capable of simulating storm surge, tides, river discharge, and rainfall can provide substantial improvement over single-hazard modeling approaches. Although the coastal-only model may be adequate to predict water levels in the waterways for storms such as Ike and Rita, which were accompanied by shorter-duration rainfall and more extreme surge, we identified overland areas where multiple drivers contributed to peak water levels for both storms, thus motivating the use of the compound model.

Our results also demonstrate that critical water and wastewater infrastructure in the region is susceptible to flooding from multiple sources, depending on the characteristics of individual tropical cyclone events. This has important implications for infrastructure planning and operation, suggesting the need for adaptation approaches that address flood hazards holistically. Incorporating projected sea-level rise and changes in tropical cyclone activity and structure is also important to ensure that the design of flood protection is adequate to address both current and future threats. Although beyond the scope of the current study, this will be the focus of follow-on work.

Overall, this study highlights the importance of characterizing the spatial and temporal influence of and interactions between coastal, fluvial, and pluvial drivers to more accurately assess flood hazards in the SNE. Although our focus here is on a single estuary in southeast Texas, the modeling approach can be applied to similar bay and estuary systems where data of adequate quantity and quality are available to evaluate the local factors that contribute to compound flood potential and to inform more comprehensive flood hazard assessment in coastal communities.

Data Availability Statement

The water level, river discharge, wind, pressure, and rainfall data sets used in this study are publicly available through the citations provided in Section 3. The topographic, bathymetric, and Manning's *n* roughness data sets used in our model are available through the Zenodo data repository at https://doi.org/10.5281/zenodo.7213729. Model outputs generated for this study are also included in the Zenodo repository.

Acknowledgments
This project was funded through the National Oceanic and Atmospheric Administration's Climate Program Office under the COCA and SARP programs (Grant NA19OAR4310347). The authors thank Md Arifur Rahman for providing some of the input data used in this project.

References

Abbaszadeh, P., Muñoz, D. F., Moftakhari, H., Jafarzadegan, K., & Moradkhani, H. (2022). Perspective on uncertainty quantification and reduction in compound flood modeling and forecasting. *Iscience*, *25*, 105201. https://doi.org/10.1016/j.isci.2022.105201

Asher, T. G., Luettich, R. A., Jr., Fleming, J. G., & Blanton, B. O. (2019). Low frequency water level correction in storm surge models using data assimilation. *Ocean Modelling*, *144*, 101483. https://doi.org/10.1016/j.ocemod.2019.101483

Bakhtyar, R., Maitaria, K., Velissariou, P., Trimble, B., Mashriqui, H., Moghimi, S., et al. (2020). A new 1D/2D coupled modeling approach for a riverine–estuarine system under storm events: Application to Delaware River basin. *Journal of Geophysical Research: Oceans*, *125*, e2019JC015822. https://doi.org/10.1029/2019JC015822

Berg, R. (2009). *National Hurricane Center Tropical Cyclone Report: Hurricane Ike* (Tech. Rep.). National Oceanic and Atmospheric Administration, National Weather Service. Retrieved from https://www.nhc.noaa.gov/data/tcr/AL092008_Ike.pdf

Bilskie, M. V., & Hagen, S. (2018). Defining flood zone transitions in low-gradient coastal regions. *Geophysical Research Letters*, *45*, 2761–2770. https://doi.org/10.1002/2018GL077524

Bilskie, M. V., Zhao, H., Resio, D., Atkinson, J., Cobell, Z., & Hagen, S. C. (2021). Enhancing flood hazard assessments in coastal Louisiana through coupled hydrologic and surge processes. *Frontiers in Water*, *3*, 609231. https://doi.org/10.3389/frwa.2021.609231

Blake, E. S., & Zelinsky, D. A. (2018). *National Hurricane Center Tropical Cyclone Report: Hurricane Harvey* (Tech. Rep.). National Oceanic and Atmospheric Administration, National Weather Service. Retrieved from https://www.nhc.noaa.gov/data/tcr/AL092017_Harvey.pdf

Brown-Giammanco, T. M., Giammanco, I. M., & Pogorzelski, H. (2018). *Hurricane Harvey wind damage investigation* (Tech. Rep.). Insurance Institute for Business & Home Safety. Retrieved from https://ibhs.org/wp-content/uploads/member_docs/Hurricane-Harvey-Wind-Damage-Investigation_IBHS.pdf

Campbell, T., Allard, R., Preller, R., Smedstad, L., Wallcraft, A., Chen, S., et al. (2010). Integrated modeling of the battlespace environment. *Computing in Science & Engineering*, *12*(5), 36–45. https://doi.org/10.1109/MCSE.2010.78

Center for Computation and Technology and Louisiana Sea Grant, Louisiana State University. (2022). Coastal Emergency Risks Assessment. Retrieved from https://coastalrisk.live/

Chen, W. B., & Liu, W. C. (2014). Modeling flood inundation induced by river flow and storm surges over a river basin. *Water*, *6*(10), 3182–3199. https://doi.org/10.3390/w6103182

Cooperative Institute for Research in the Atmosphere. (2021). The tropical cyclone extended best track dataset (EBTRK): Atlantic basin dataset 1851 to 2020 [Dataset]. Cooperative Institute for Research in the Atmosphere. Retrieved from https://rammb2.cira.colostate.edu/wp-content/uploads/2020/11/EBTRK_AL_final_1851-2020_new_format_v3.0.1_23-Aug-2021.txt

Copeland, C. (2005). *Hurricane-damaged drinking water and wastewater facilities: Impacts, needs, and response* (Tech. Rep.). Congressional Research Service. Retrieved from https://www.everycrsreport.com/files/20051019_RS22285_9e256f667588ee1b362d6a4054676b20fb14fdd3.pdf

Couasnon, A., Sebastian, A., & Morales-Nápoles, O. (2018). A copula-based Bayesian network for modeling compound flood hazard from riverine and coastal interactions at the catchment scale: An application to the Houston Ship Channel, Texas. *Water*, *10*(9), 1190. https://doi.org/10.3390/w10091190

Dartmouth Flood Observatory. (2019). DFO flood event: 2019-USA-4797. Retrieved from http://floodobservatory.colorado.edu/Events/4797/2019USA4797.html

Deltares. (2020). Delft3D Flexible Mesh Suite. Retrieved from https://www.deltares.nl/en/software/delft3d-flexible-mesh-suite/

Deltares. (2022). *Delft3D Hydro-Morphodynamics User Manual* (Tech. Rep.). Retrieved from https://content.oss.deltares.nl/delft3d/manuals/Delft3D-FLOW_User_Manual.pdf

Dietrich, J. C., Tanaka, S., Westerink, J. J., Dawson, C. N., Luettich, R., Zijlema, M., et al. (2012). Performance of the unstructured-mesh, SWAN+ADCIRC model in computing hurricane waves and surge. *Journal of Scientific Computing*, *52*(2), 468–497. https://doi.org/10.1007/s10915-011-9555-6

Ebad Sichani, M., Anarde, K. A., Capshaw, K. M., Padgett, J. E., Meidl, R. A., Hassanzadeh, P., et al. (2020). Hurricane risk assessment of petroleum infrastructure in a changing climate. *Frontiers in Built Environment*, *6*, 104. https://doi.org/10.3389/fbuil.2020.00104

Emanuel, K. (2005). Increasing destructiveness of tropical cyclones over the past 30 years. *Nature*, *436*(7051), 686–688. https://doi.org/10.1038/nature03906

Emanuel, K. (2013). Downscaling CMIP5 climate models shows increased tropical cyclone activity over the 21st century. *Proceedings of the National Academy of Sciences of the United States of America*, *110*(30), 12219–12224. https://doi.org/10.1073/pnas.1301293110

Emanuel, K. (2017). Assessing the present and future probability of Hurricane Harvey's rainfall. *Proceedings of the National Academy of Sciences of the United States of America*, *114*(48), 12681–12684. https://doi.org/10.1073/pnas.1716222114

Federal Emergency Management Agency. (2016). *Guidance for flood risk analysis and mapping: Coastal water levels* (Tech. Rep.). Retrieved from https://www.fema.gov/sites/default/files/2020-02/Coastal_Water_Levels_Guidance_May_2016.pdf

Federal Emergency Management Agency & US Army Corps of Engineers. (2011). *Flood insurance study: Coastal counties, Texas. Intermediate submission 2: Scoping and data review* (Tech. Rep.).

Goodall, J. L., Robinson, B. F., & Castronova, A. M. (2011). Modeling water resource systems using a service-oriented computing paradigm. *Environmental Modelling & Software*, *26*(5), 573–582. https://doi.org/10.1016/j.envsoft.2010.11.013

Gori, A., Lin, N., & Smith, J. (2020). Assessing compound flooding from landfalling tropical cyclones on the North Carolina coast. *Water Resources Research*, *56*, e2019WR026788. https://doi.org/10.1029/2019WR026788

Gori, A., Lin, N., & Xi, D. (2020). Tropical cyclone compound flood hazard assessment: From investigating drivers to quantifying extreme water levels. *Earth's Future*, *8*, e2020EF001660. https://doi.org/10.1029/2020EF001660

Herdman, L., Erikson, L., & Barnard, P. (2018). Storm surge propagation and flooding in small tidal rivers during events of mixed coastal and fluvial influence. *Journal of Marine Science and Engineering*, *6*(4), 158. https://doi.org/10.3390/jmse6040158

Hinkel, J., Lincke, D., Vafeidis, A. T., Perrette, M., Nicholls, R. J., Tol, R. S., et al. (2014). Coastal flood damage and adaptation costs under 21st century sea-level rise. *Proceedings of the National Academy of Sciences of the United States of America*, *111*(9), 3292–3297. https://doi.org/10.1073/pnas.1222469111

Hsu, M.-H., Kuo, A. Y., Kuo, J.-T., & Liu, W.-C. (1999). Procedure to calibrate and verify numerical models of estuarine hydrodynamics. *Journal of Hydraulic Engineering*, *125*(2), 166–182. https://doi.org/10.1061/(ASCE)0733-9429(1999)125:2(166)

Huang, W., Ye, F., Zhang, Y. J., Park, K., Du, J., Moghimi, S., et al. (2021). Compounding factors for extreme flooding around Galveston bay during hurricane Harvey. *Ocean Modelling*, *158*(804), 1–35. https://doi.org/10.1016/j.ocemod.2020.101735

Iowa Environmental Mesonet. (2022). Multi-Radar Multi-Sensor Data Respository. Retrieved from https://mtarchive.geol.iastate.edu/2017/

Karamouz, M., Razmi, A., Nazif, S., & Zahmatkesh, Z. (2017). Integration of inland and coastal storms for flood hazard assessment using a distributed hydrologic model. *Environmental Earth Sciences*, *76*(11), 1–17. https://doi.org/10.1007/s12665-017-6722-6

Knabb, R. D., Brown, D. P., & Rhome, J. R. (2006). *National Hurricane Center Tropical Cyclone Report: Hurricane Rita* (Tech. Rep.). National Oceanic and Atmospheric Administration, National Weather Service. Retrieved from https://www.nhc.noaa.gov/data/tcr/AL182005_Rita.pdf

Kumbier, K., Carvalho, R. C., Vafeidis, A. T., & Woodroffe, C. D. (2018). Investigating compound flooding in an estuary using hydrodynamic modelling: A case study from the Shoalhaven River, Australia. *Natural Hazards and Earth System Sciences*, *18*(2), 463–477. https://doi.org/10.5194/nhess-18-463-2018

Liu, F. (2017). *Analyzing the influence of compound events on flooding in the downstream reach of the Houston Ship Channel*. Delft University of Technology.

Loveland, M., Kiaghadi, A., Dawson, C. N., Rifai, H. S., Misra, S., Mosser, H., & Parola, A. (2021). Developing a modeling framework to simulate compound flooding: When storm surge interacts with riverine flow. *Frontiers in Climate*, *2*, 609610. https://doi.org/10.3389/fclim.2020.609610

Lower Neches Valley Authority. (2018). *Stakeholder update: The Texas clean rivers program* (Tech. Rep.). Retrieved from https://lnva.dst.tx.us/wp-content/uploads/2018/09/05162018-CRP-Stakeholder-Newsletter-FINAL.pdf

Mejia Manrique, S. A., Harmsen, E. W., Khanbilvardi, R. M., & González, J. E. (2021). Flood impacts on critical infrastructure in a coastal floodplain in Western Puerto Rico during hurricane María. *Hydrology*, *8*(3), 104. https://doi.org/10.3390/hydrology8030104

Muis, S., Verlaan, M., Winsemius, H. C., Aerts, J. C., & Ward, P. J. (2016). A global reanalysis of storm surges and extreme sea levels. *Nature Communications*, *7*(1), 1–12. https://doi.org/10.1038/ncomms11969

Muñoz, D. F., Abbaszadeh, P., Moftakhari, H., & Moradkhani, H. (2022a). Accounting for uncertainties in compound flood hazard assessment: The value of data assimilation. *Coastal Engineering*, *171*, 104057. https://doi.org/10.1016/j.coastaleng.2021.104057

Muñoz, D. F., Moftakhari, H., Kumar, M., & Moradkhani, H. (2022b). Compound effects of flood drivers, sea level rise, and dredging protocols on vessel navigability and wetland inundation dynamics. *Frontiers in Marine Science*, *9*, 906376. https://doi.org/10.3389/fmars.2022.906376

Muñoz, D. F., Moftakhari, H., & Moradkhani, H. (2020). Compound effects of flood drivers and wetland elevation correction on coastal flood hazard assessment. *Water Resources Research*, *56*, e2020WR027544. https://doi.org/10.1029/2020WR027544

Naseri, K., & Hummel, M. (2022). A Bayesian copula-based nonstationary framework for compound flood risk assessment along US coastlines. *Journal of Hydrology*, *610*, 128005. https://doi.org/10.1016/j.jhydrol.2022.128005

National Center for Atmospheric Research. (2017). The climate data guide: CCMP: Cross-calibrated multi-platform wind vector analysis. Retrieved from https://climatedataguide.ucar.edu/climate-data/ccmp-cross-calibrated-multi-platform-wind-vector-analysis

National Center for Atmospheric Research. (2022). Research data archive: Computational and information system lab [Dataset]. National Center for Atmospheric Research. Retrieved from https://rda.ucar.edu/datasets/ds608.0/index.html%23cgi%2Dbin/datasets/

National Oceanic and Atmospheric Administration. (2013). *Tide prediction error for the United States stations* (Tech. Rep.). Retrieved from https://tidesandcurrents.noaa.gov/pdf/Tide_Prediction_Error_for_the_United_States_Coastline.pdf

National Oceanic and Atmospheric Administration. (2022a). Billion-dollar weather and climate disasters. Retrieved from https://www.ncdc.noaa.gov/billions/summary%2Dstats%23temporal%2Dcomparison%2Ddiv

National Oceanic and Atmospheric Administration. (2022b). Index of Analysis of Record for Calibration: Historic. Retrieved from https://hydrology.nws.noaa.gov/aorc-historic/

National Oceanic and Atmospheric Administration. (2022c). Sea, Lake, and Overland Surges from Hurricanes (SLOSH). Retrieved from https://www.nhc.noaa.gov/surge/slosh.php

National Oceanic and Atmospheric Administration. (2022d). Tides and currents. Retrieved from https://tidesandcurrents.noaa.gov

National Science Foundation. (2019). Hydroshare THREDDS service: Dataset [Dataset]. NSF. Retrieved from https://thredds.hydroshare.org/thredds/catalog/catalog.html

National Weather Service. (2017). Hurricane Harvey and its impacts on southeast Texas (August 25–29, 2017). Retrieved from https://www.weather.gov/hgx/hurricaneharvey

Santiago-Collazo, F. L., Bilskie, M. V., Bacopoulos, P., & Hagen, S. C. (2021). An examination of compound flood hazard zones for past, present, and future low-gradient coastal land-margins. *Frontiers in Climate*, *3*, 684035. https://doi.org/10.3389/fclim.2021.684035

Santiago-Collazo, F. L., Bilskie, M. V., & Hagen, S. C. (2019). A comprehensive review of compound inundation models in low-gradient coastal watersheds. *Environmental Modelling & Software*, *119*, 166–181. https://doi.org/10.1016/j.envsoft.2019.06.002

Santos, V. M., Wahl, T., Jane, R., Misra, S. K., & White, K. D. (2021). Assessing compound flooding potential with multivariate statistical models in a complex estuarine system under data constraints. *Journal of Flood Risk Management*, *14*(4), e12749. https://doi.org/10.1111/jfr3.12749

Schwab, K. J., Gibson, K. E., Williams, D. L., Kulbicki, K. M., Lo, C. P., Mihalic, J. N., et al. (2007). Microbial and chemical assessment of regions within New Orleans, LA impacted by Hurricane Katrina. *Environmental Science & Technology*, *41*(7), 2401–2406. https://doi.org/10.1021/es062916x

Sebastian, A., Bader, D., Nederhoff, C., Leijnse, T., Bricker, J., & Aarninkhof, S. (2021). Hindcast of pluvial, fluvial, and coastal flood damage in Houston, Texas during Hurricane Harvey (2017) using SFINCS. *Natural Hazards*, *109*(3), 2343–2362. https://doi.org/10.1007/s11069-021-04922-3

Silva-Araya, W. F., Santiago-Collazo, F. L., Gonzalez-Lopez, J., & Maldonado-Maldonado, J. (2018). Dynamic modeling of surface runoff and storm surge during hurricane and tropical storm events. *Hydrology*, *5*(1), 1–28. https://doi.org/10.3390/hydrology5010013

Sobel, A. H., Camargo, S. J., Hall, T. M., Lee, C.-Y., Tippett, M. K., & Wing, A. A. (2016). Human influence on tropical cyclone intensity. *Science*, *353*(6296), 242–246. https://doi.org/10.1126/science.aaf6574

Sulis, M., Meyerhoff, S. B., Paniconi, C., Maxwell, R. M., Putti, M., & Kollet, S. J. (2010). A comparison of two physics-based numerical models for simulating surface water–groundwater interactions. *Advances in Water Resources*, *33*(4), 456–467. https://doi.org/10.1016/j.advwatres.2010.01.010

Sweet, W. V., & Park, J. (2014). From the extreme to the mean: Acceleration and tipping points of coastal inundation from sea level rise. *Earth's Future*, *2*, 579–600. https://doi.org/10.1002/2014EF000272

Tang, H. S., Chien, S. I., Temimi, M., Blain, C. A., Ke, Q., Zhao, L., & Kraatz, S. (2013). Vulnerability of population and transportation infrastructure at the east bank of Delaware Bay due to coastal flooding in sea-level rise conditions. *Natural Hazards*, *69*(1), 141–163. https://doi.org/10.1007/s11069-013-0691-1

Thyng, K. M., Hetland, R. D., Socolofsky, S. A., Fernando, N., Turner, E. L., & Schoenbaechler, C. (2020). Hurricane Harvey caused unprecedented freshwater inflow to Galveston Bay. *Estuaries and Coasts*, *43*(7), 1836–1852. https://doi.org/10.1007/s12237-020-00800-6

Trenberth, K. E., Cheng, L., Jacobs, P., Zhang, Y., & Fasullo, J. (2018). Hurricane Harvey links to ocean heat content and climate change adaptation. *Earth's Future*, *6*, 730–744. https://doi.org/10.1029/2018EF000825

United States Census Bureau. (2021). Quickfacts. Retrieved from https://www.census.gov/quickfacts/fact/table/beaumontcitytexas,US/HSG650219

U.S. Environmental Protection Agency. (2019). EPA region 6 quickly assessed water infrastructure after Hurricane Harvey but can improve emergency outreach to disadvantaged communities. Retrieved from https://www.epa.gov/sites/default/files/2019-07/documents/_epao-ig_20190716_19-p-0236.pdf

U.S. Geological Survey. (2010). Enhanced National Land Cover Data 1992 (NLCDe 92) [Dataset]. Retrieved from https://water.usgs.gov/GIS/metadata/usgswrd/XML/nlcde92.xml

U.S. Geological Survey. (2011). Discharge measurement quality code. Retrieved from https://help.waterdata.usgs.gov/codes-and-parameters/discharge-measurement-quality-code

U.S. Geological Survey. (2022a). Flood event viewer. Retrieved from https://stn.wim.usgs.gov/FEV/%232017Harvey

U.S. Geological Survey. (2022b). National water information system: Web interface. Retrieved from https://waterdata.usgs.gov/nwis/inventory?agency_code=USGS%26site_no=08041780

Veeramony, J., Condon, A., & van Ormondt, M. (2017). Forecasting storm surge and inundation: Model validation. *Weather and Forecasting*, *32*(6), 2045–2063. https://doi.org/10.1175/waf-d-17-0015.1

Wasileski, G., Rodríguez, H., & Diaz, W. (2011). Business closure and relocation: A comparative analysis of the Loma Prieta earthquake and Hurricane Andrew. *Disasters*, *35*(1), 102–129. https://doi.org/10.1111/j.1467-7717.2010.01195.x

Wing, O. E., Sampson, C. C., Bates, P. D., Quinn, N., Smith, A. M., & Neal, J. C. (2019). A flood inundation forecast of Hurricane Harvey using a continental-scale 2D hydrodynamic model. *Journal of Hydrology*, *4*, 100039. https://doi.org/10.1016/j.hydroa.2019.100039

Wuebbles, D. J., Fahey, D. W., & Hibbard, K. A. (2017). *Climate Science Special Report: Fourth National Climate Assessment Volume I* (Tech. Rep.). https://doi.org/10.7930/J0J964J6

Xiao, Z., Yang, Z., Wang, T., Sun, N., Wigmosta, M., & Judi, D. (2021). Characterizing the non-linear interactions between tide, storm surge, and river flow in the Delaware Bay Estuary, United States. *Frontiers in Marine Science*, *8*, 715557. https://doi.org/10.3389/fmars.2021.715557

Ye, F., Huang, W., Zhang, Y. J., Moghimi, S., Myers, E., Pe'eri, S., & Yu, H. C. (2021). A cross-scale study for compound flooding processes during Hurricane Florence. *Natural Hazards and Earth System Sciences*, *21*(6), 1703–1719. https://doi.org/10.5194/nhess-21-1703-2021

Ye, F., Zhang, Y. J., Yu, H., Sun, W., Moghimi, S., Myers, E., et al. (2020). Simulating storm surge and compound flooding events with a creek-to-ocean model: Importance of baroclinic effects. *Ocean Modelling*, *145*, 101526. https://doi.org/10.1016/j.ocemod.2019.101526

Zhang, Y., & Najafi, M. R. (2020). Probabilistic numerical modeling of compound flooding caused by tropical storm Matthew over a data-scarce coastal environment. *Water Resources Research*, *56*, e2020WR028565. https://doi.org/10.1029/2020WR028565

Zhang, Y. J., Ye, F., Yu, H., Sun, W., Moghimi, S., Myers, E., et al. (2020). Simulating compound flooding events in a hurricane. *Ocean Dynamics*, *70*(5), 621–640. https://doi.org/10.1007/s10236-020-01351-x

Zscheischler, J., Westra, S., Van Den Hurk, B. J., Seneviratne, S. I., Ward, P. J., Pitman, A., et al. (2018). Future climate risk from compound events. *Nature Climate Change*, *8*(6), 469–477. https://doi.org/10.1038/s41558-018-0156-3